JOURNAL OF PETROLOGY | VOLUME 37 | NUMBER 1 | PAGES 45–71 | 1996

S. TURNER[1]*, N. ARNAUD[2], J. LIU[3], N. ROGERS[1], C. HAWKESWORTH[1], N. HARRIS[1], S. KELLEY[1], P. VAN CALSTEREN[1] AND W. DENG[3]

[1]DEPARTMENT OF EARTH SCIENCES, THE OPEN UNIVERSITY, MILTON KEYNES MK7 6AA, UK

[2]UNIVERSITÉ BLAISE PASCAL ET URA 10 CNRS, 5 KESSLER, 63038 CLERMONT-FERRAND CEDEX, FRANCE

[3]INSTITUTE OF GEOLOGY, ACADEMIA SINICA, P.O. BOX 634, BEIJING 100011, PEOPLE'S REPUBLIC OF CHINA

Post-collision, Shoshonitic Volcanism on the Tibetan Plateau: Implications for Convective Thinning of the Lithosphere and the Source of Ocean Island Basalts

Potassic volcanism has been widespread and semi-continuous on the Tibetan plateau since ~13 Ma, post-dating the orogenic thickening of the India–Asia collision. Volcanism may have commenced slightly earlier (~16–20 Ma) in the southern portion of the plateau and then ceased around 10 Ma. The dominant lavas are pyroxene- and plagioclase-phyric shoshonites with subordinate occurrences of dacites and rhyolites. Their mineralogy reflects crystallization from high-temperature (≤1100°C) magmas which had elevated oxygen and water fugacities. Geochemically, they are characterized by relatively low TiO_2, Al_2O_3 and Fe_2O_3, and high Na_2O, coupled with variable abundances of compatible trace elements and very high contents of incompatible trace elements. Normalized incompatible element patterns have marked negative Nb, Ta and Ti anomalies whereas K_2O appears to be buffered at ~4% over a wide range of SiO_2. Isotope data show a relatively broad and enriched range of $^{87}Sr/^{86}Sr$ (0·7076–0·7106) at more restricted ε_{Nd} (−5·2 to −8·1). Pb isotopes are characterized by a range of $^{207}Pb/^{204}Pb$ (15·51–15·72) and $^{208}Pb/^{204}Pb$ (38·67–39·30) at very uniform $^{206}Pb/^{204}Pb$ (18·39–18·83), leading to vertical arrays. Volcanics from the southern parts of the plateau have more primitive isotopic compositions: $^{87}Sr/^{86}Sr$ 0·7048–0·7080, ε_{Nd} 1·4 to −3·3, $^{206}Pb/^{204}Pb$ 18·48–18·67, $^{207}Pb/^{204}Pb$ 15·59–15·68 and $^{208}Pb/^{204}Pb$ 38·73–38·98.

In general, the geochemical and isotopic data most closely approximate partial melting arrays, although fractionation processes have clearly operated. The isotopic ratios and the enrichment of incompatible elements and LREE/HREE cannot be derived from a depleted mantle source via a single-stage melting process. Instead, a metasomatized, garnet peridotite source containing ~6% phlogopite is required and this is inferred to lie within the lithospheric mantle. The enrichment in incompatible elements in this source must have been sufficiently ancient to generate the observed isotopic ratios, and Nd depleted mantle model ages suggest this was Proterozoic in age (~1·2 Ga), whereas Pb model ages record an Archaean event, suggesting the source had a multi-stage enrichment history. The negative Ta, Nb and Ti anomalies and low Rb/Ba suggest that metasomatism may have occurred during an ancient subduction episode. The high $^{208}Pb/^{204}Pb$, $^{207}Pb/^{204}Pb$ and low Nb/U, Ce/Pb of the Tibetan shoshonites are distinct from ocean island basalts. Thus, if convectively removed lithospheric mantle provides a source for ocean island basalts, it must differ significantly from the source of the Tibetan shoshonites.

A lithospheric mantle source for the volcanism places important constraints on geodynamic models for the evolution of the Tibetan plateau and the India–Asia collision. For likely thermal structures beneath the plateau, the temperatures required to trigger melting within the lithospheric mantle can only be plausibly obtained if the lower parts of the lithospheric mantle were removed by convective thinning. This is consistent with recent models which invoke the same process to explain the current elevation and extensional deformation of the plateau. The age data suggest this occurred at ~13 Ma and the duration of volcanism may be explained by continued conductive heating since that time. Poorly sampled but slightly older volcanics from the southern portions of the plateau may indicate that convective thinning began in the south and migrated northwards. Rapid

*Corresponding author.

uplift of the plateau may have resulted in increased rates of chemical weathering, which led to global cooling, as indicated by oxygen isotope data from Atlantic sediments.

KEY WORDS: *climate; lithospheric mantle; OIB; Tibet; volcanism*

INTRODUCTION

The India–Asia collision and the resultant Himalaya provides the best modern example of continental collision plate tectonics. Associated with the development of this orogen, and formed as a consequence of the continuing indentation of India into Asia, is the problematic Tibetan plateau, which has had a central role in the development of recent models for the mechanics of mountain belts (e.g. England & Houseman, 1988, 1989) and Cenozoic climate change (e.g. Raymo & Ruddiman, 1992; Kutzbach *et al.*, 1993). The evolving tectonic regimes of orogenic belts are typically marked by changes in the composition of associated magmatism, and the India–Asia collision has provided a type example of the progression through geochemically distinctive pre-, syn- and post-collision magmatism (Harris *et al.*, 1986). Post-collision, potassic magmatism is a common feature in many collisional orogens around the world and, although in a thermal context its origin is poorly understood, it often has similar characteristics irrespective of location and age (Pearce *et al.*, 1984; Harris *et al.*, 1986; Turner *et al.*, 1992). Clearly, the potassic volcanism that post-dates collision, and is still active on the Tibetan plateau today, provides a potentially important window into the deep thermal and compositional structure of the India–Asia orogen.

Various earlier studies have documented the existence of the Tibetan post-collision volcanism (e.g. Coulon *et al.*, 1986; Pearce & Mei, 1988; Deng, 1989*a*, 1989*b*; Liu & Maimaiti, 1989; Arnaud *et al.*, 1992; Turner *et al.*, 1993); however, most have provided only limited analytical data. To provide the first comprehensive data set we include these data and additionally, analyses of samples collected by W. M. Deng during the 1987–1988 Academia Sinica field expeditions, samples collected by J. Liu and samples collected by N. Arnaud during the 1989–1990 Sino-French geotraverses. In conjunction with data published by McKenna & Walker (1990) and Coulon *et al.* (1986), this constitutes all available data to our knowledge. The volcanic rocks are first described according to age, location and composition, then the constraints on their source region are discussed. Finally, these observations are used to assess this volcanism in the context of geodynamic models for the evolution of the India–Asia collision and the Tibetan plateau and the source regions of ocean island basalts.

GEOLOGICAL SETTING

The Tibetan plateau forms the most prominent topographic structure on Earth. Surrounded by high-altitude ranges on all sides except to the east, its average altitude exceeds 5000 m over an area greater than 10^6 km^2. The plateau is bounded to the north by the Tarim basin, and to the south by the Himalaya (extending to the west in Pakistan as the Karakorum range). The structure of the plateau is one of a tectonic collage of continental blocks accreted to the southern margin of Eurasia during successive ocean basin closures since the Permian. From north to south, the four main crustal blocks are Kunlun, Songban-Ganzi, Qiangtang and Lhasa, with the broadly accepted ages for these collisional events being late Permian for Kunlun–Songban, late Triassic to early Jurassic for Songban–Qiantang and late Jurassic for Qiangtang–Lhasa (Dewey *et al.*, 1988). In the present tectonic setting these blocks are disrupted by the sinistral strike slip Altyn-Tagh fault marking the northern limit of Tibet and western limit of the Kunlun block, and the dextral strike slip Karakorum fault to the south and west (Fig. 1).

Successive stages of the India–Asia collision and accretion of the Tibetan plateau were accompanied by specific magmatic associations. During the Cretaceous and Palaeocene, India moved northwards towards Asia via subduction of Tethyan oceanic crust beneath Asia. This was accompanied by voluminous calc-alkaline arc magmatism from ~120 to 50 Ma (Debon *et al.*, 1986; Harris *et al.*, 1988*a*, 1988*b*; Pearce & Mei, 1988), now exposed parallel to, and just north of the main mantle thrust which lies at the southern edge of the Tibetan plateau. Continental collision started in the Early Tertiary (~55 Ma) to the west (in Pakistan) and spread progressively toward the east. The absence of any oceanic basin remnants after 50 Ma, and the decrease in speed of the northward drift of India, show that continental collision was under way along the whole southern margin of Eurasia by that time, involving crustal thickening, obduction of oceanic crust and partial underthrusting of the Indian continent beneath Asia. During the last 50 Ma, India has moved northwards with respect to Asia at a constant rate (4–5 cm/yr) indenting Asia by >2000 km. This has apparently been accommodated by internal deformation (Houseman & England, 1994; Jin *et al.*, 1994; Hirn *et al.*, 1995) of India and Asia and formation of the Tibetan plateau. A second pulse of magmatism, recorded by crustally derived peraluminous leuco-

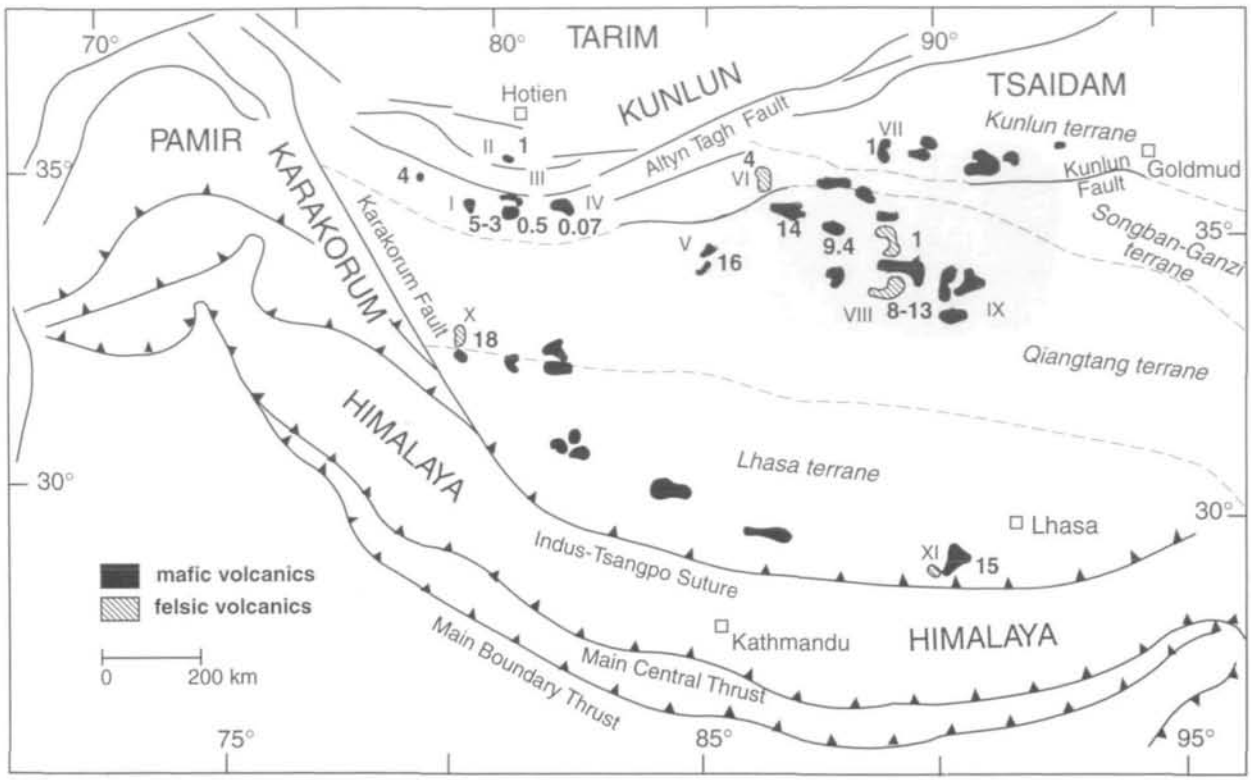

Fig. 1. General map of the India–Eurasia collision zone and Tibetan Plateau, showing the terranes (dashed lines) which make up the plateau, the area of high mantle temperatures inferred from seismic data (shaded region) and the distribution of potassic volcanism [modified from Arnaud (1992) and based on remote sensing data from Spot and Landsat images as well as the China geological map from the Academia Sinica]. Ages [from Tables 1 and 2; 4 Ma age for Ulugh Muztagh (area VI) from Burchfiel *et al.* (1989)] are shown in heavy numerals, sub-areas in roman numerals. The sub-areas can be grouped into a northwestern region (areas I–IV), a northeastern region (areas V–IX) and a southern region (areas X and XI).

granites (e.g. France-Lanord & Le Fort, 1988; Harris & Massey, 1994) emplaced at ~20 Ma in the central High Himalaya most probably reflects increasing temperatures in the thickened crust coupled with decompression (e.g. Harris & Massey, 1994) that has been associated with the onset of rapid exhumation of the Himalaya (e.g. Copeland *et al.*, 1987, 1990; Burchfiel *et al.*, 1989).

In contrast to the Himalaya, the central Tibetan plateau was generally devoid of magmatic activity between 90 Ma and the Mid-Miocene, since which time it has become the site of widespread (Fig. 1), but small volume, eruptions of potassic basalts and lesser felsic lavas (e.g. Coulon *et al.*, 1986; Pearce & Mei, 1988; Liu & Maimaiti, 1989; McKenna & Walker, 1990; Arnaud *et al.*, 1992; Turner *et al.*, 1993). The southern plateau preserves Cretaceous to Early Eocene fossiliferous limestones, indicating it was at sea-level before collision (Norin, 1946; Li *et al.*, 1981), and a Mid- to Late Miocene pediplain indicating a lack of exhumation since that time (Shackelton & Chang, 1988). Seismic data indicate that the crust of the plateau has since been thickened to approximately twice normal thickness (~70 km) although considerable lateral thickness variations are inferred (Molnar, 1990). Low shear-wave velocities and high attenuation indicate that the north–central part of the plateau, where the crust is thinnest (50–60 km), is underlain by anomalously hot mantle and here Moho temperatures may approach 1000°C (Brandon & Romanovitz, 1986; Molnar, 1988). Importantly, the plateau is currently undergoing east–west extension (~1%/m.y.) on north–south normal faults despite the continuing convergence of India and Asia (Armijo *et al.*, 1986; Mercier *et al.*, 1987; Kidd & Molnar, 1988; Maluski *et al.*, 1988; Pan & Kidd, 1992; Coleman & Hodges, 1995). Tertiary thrust faults indicate that the plateau was under compression for most of the Tertiary and extension appears to have commenced around 14–10 Ma (Mercier *et al.*, 1987; Maluski *et al.*, 1988; Pan & Kidd, 1992; Coleman & Hodges, 1995).

AGE AND GEOGRAPHIC DISTRIBUTION OF THE LAVAS

The distribution of potassic volcanic samples obtained from the Tibetan plateau is divided into 11 sub-areas in Fig. 1. In detail, volcanism crosses several major tectonic and morphologic terranes and is rarely associated with clear tectonic structures, such as grabens or normal faulting. Exceptions are the Ashikule area (IV) and the Ulugh Muztagh area (VI), which seem to occupy large pull-apart basins. To simplify the remaining discussion, the 11 areas are grouped into three large geographical regions, two in the north and one in the south (see Fig. 1). Areas I–IV make up the northwestern region, whereas the greatest concentration of volcanism is located in the central northeastern region (areas V–IX), where high mantle temperatures and the presence of partial melt are inferred from inefficient S_n wave propagation (Molnar, 1988; Hirn *et al.*, 1995). Finally, the volcanics from the southern plateau are represented by the Shiquanhe (area X) and Maquiang (area XI) volcanics.

Table 1 summarizes the existing age data which, with the exception of the work of Coulon *et al.* (1986), largely employed the K–Ar method. As part of this study, new laser whole-rock fusion ^{40}Ar–^{39}Ar age data were obtained on lavas from the north–central part of the plateau where few age data were previously available. The data fall within the age range of the existing data but are concentrated around 8–13 Ma (Table 2). Combining these data with those already in the literature, and excluding for the moment data from the southern part of the plateau, and one K–Ar age of 16 Ma in area V, the data span a period from 13 Ma to the present; an eruption occurred in the Ashikule area in 1951 (Liu & Maimaiti, 1989). There appears to be little systematic geographical distribution to the volcanism and although no age older than 5 Ma is recorded in the northwestern region, young deposits are found throughout the northern plateau. Locally mafic and silicic volcanics are sometimes associated in a restricted area (areas I or VIII, for example) and where these have been dated they showed roughly the same age, implying bimodal volcanism. Owing to the limited age data available it is not possible to interpret any pattern to the intensity of this volcanism.

Although the data are limited, there is some suggestion that volcanism commenced (and apparently ceased) earlier in the southern parts of the plateau, with no ages younger than 10 Ma yet recorded; Coulon *et al.* (1986) reported ^{40}Ar–^{39}Ar step heating ages on mineral separates from lavas in the Maquiang area (XI) near Lhasa that range from 10 to 16 Ma, whereas K–Ar ages on intermediate-silicic volcanics from the Shiquanhe area (X) in the southwest lie in the range 16–20 Ma (Table 1). This apparent northward younging is shown diagrammatically in Fig. 15a, below; unfortunately, despite the occurrence of numerous volcanic fields in the central southern part of the plateau (Fig. 1), there are as yet no samples or age data to confirm the duration of volcanism in these southern parts of the plateau. Collection of such samples is now a high priority.

Table 1: Published K–Ar age determinations on Tibetan lavas

Sample no.	Location	Age	Reference
K89G185	I	5·6	1
K89G197	I	6·4	1
K89G200	I	3·6	1
Kp 23-1	II	1·2	2
Kp 24-1	III	2–0·2	2
k713	IV	0·4	3
k716	IV	0·2	3
k718	IV	0·3	3
k720	IV	0·7	3
k723	IV	0·6	3
K732	IV	0·3	3
K738	IV	0·6	3
Kp 12-4	IV	0·07	2
kp 10-3	V	16	2
Bg 121	VI	14	2
Kp 35-10	VII	1·07	2
COUL 328	XI	Oct-16	4
K89G159	X	16	1
K89G162	X	18	1
K89G163	X	20	1

1, Arnaud (1992); Arnaud *et al.* (1992). 2, Deng (1989*b*). 3, Liu & Maimaiti (1989). 4, Coulon *et al.* (1986).

PETROLOGY

The morphology of eruptive centres and units varies considerably, from numerous perfectly preserved cinder cones to highly eroded pyroclastic deposits (Fig. 2a). Well-preserved maars and large collapse structures associated with pyroclastic flows have tentatively been recognized on satellite images. The volcanics are undeformed and some are interstratified with recent clastic alluvial deposits, as is

Table 2: New laser Ar–Ar whole-rock age determinations on Tibetan lavas

Sample	Location	$^{39}Ar^{a}$	Ca/K	% $^{40}Ar^{*}$	$^{40}Ar^{*}/^{39}Ar$	±	Age (Ma)	±
k9006	VIII	4·275	0·56	70	56·90	1·38	8·7	0·2
k9006	VIII	4·448	0·66	70	58·36	1·39	9·0	0·2
k9007	VIII	5·308	0·75	37	76·66	1·75	11·7	0·3
k9007	VIII	3·984	1·00	38	98·13	2·31	15·0	0·4
k9008	VIII	7·088	0·56	96	61·76	0·76	9·4	0·1
k9008	VIII	5·152	0·54	97	61·49	1·11	9·3	0·2
k9010	VIII	3·217	0·60	25	62·42	2·15	9·4	0·3
k9010	VIII	4·880	0·78	17	59·75	2·96	9·0	0·4
k9016	VIII	5·088	0·64	83	56·17	0·64	8·4	0·1
k9016	VIII	11·819	0·67	84	56·75	0·63	8·5	0·1
k9016	VIII	9·270	0·59	84	55·13	0·68	8·3	0·1
k9018	VIII	4·670	0·69	19	66·20	1·91	9·9	0·3
k9018	VIII	4·473	0·76	21	63·64	1·61	9·5	0·2
k9021	VIII	3·537	0·63	64	57·36	1·13	8·5	0·2
k9021	VIII	4·595	0·67	72	56·88	1·13	8·5	0·2
k9024	IX	5·879	1·10	22	88·12	2·93	13·0	0·4
k9024	VII	3·290	0 64	40	86·99	2·79	12·9	0·4
k9026	VII	4·651	0·93	84	87·73	1·03	12·9	0·2
k9026	VII	9 102	0·70	85	84·49	0·73	12·4	0·1
k9028	VII	4 398	1·57	31	130·14	4·15	18·5	0·6
k9031	VII	4 930	0·69	83	83·29	0·88	11·9	0·1
k9031	VII	7·267	0·77	73	80·89	0·77	11·6	0·1
k9032	VII	4·467	0·81	97	81 83	1·08	11·8	0·2
k9032	VII	10·429	0·71	94	82·70	0·58	11·9	0·1
k9038	VII	5·080	4·24	19	66·45	9·24	9·6	1·3
k9039	VII	5·174	1·19	57	85 97	1·88	12·5	0·3

[a] ^{39}Ar amounts in 10e–12 cm^3 STP.
J values were not optimized for samples with these ages. When initially analysed, these samples were expected to be Quaternary in age, in common with other samples in the north of Tibet. Selected older samples were re-irradiated at higher flux and yielded ages within error of those shown above.

the case in the Karakax valley, for example, in area I (Arnaud, 1992). The more silicic lavas are preserved as tuffs and volcanic plugs.

Despite being scattered over a vast area, the volcanics show a striking uniformity of textural and mineralogical features. The mafic lavas display typical quench textures, with abundant phenocrysts (10–40%) embedded in a fine groundmass (Fig. 2b). Glass is rarely preserved and the groundmass consists of microcrystalline feldspar, alkali feldspar, pyroxene and Fe–Ti oxides. Plagioclase, aggregated clinopyroxene and subordinate orthopyroxene are the ubiquitous phenocryst phases, along with more minor Fe–Ti oxides and rare biotite. The most undersaturated lavas contain olivine and feldspathoids (Coulon *et al.*, 1986; Deng, 1989*a*), whereas the more silicic lavas contain quartz phenocrysts and sanidine in addition to andesine and occasional biotite, and their groundmass consists essentially of alkali feldspar and quartz. The Ulugh Muztagh rhyolites (area VI) (Burchfiel *et al.*, 1989; McKenna & Walker, 1990) display rarer mineralogies including quartz, biotite and tourmaline.

Compositional data on phenocrysts from representative mafic samples ($SiO_2 = 55–58\%$) are given in Tables 3–7 and used in the following discussion. Olivine phenocrysts have *mg*-number ~83 (Table 3). Clinopyroxene phenocrysts are mostly unzoned magnesian augites (*mg*-number ~0·74) with high Al/Ti ratios, whereas the orthopyroxenes are hypersthenes (Table 4). Feldspar phenocrysts show a large compositional range from labradorite to andesine and sanidine (Table 5) and exhibit prominent compositional zonation. Oxides consist of ilmenite and

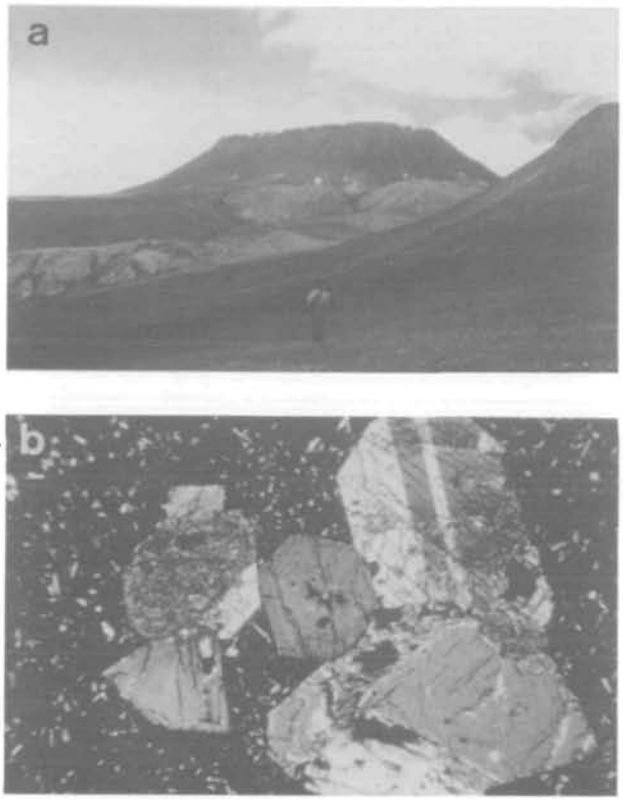

Fig. 2. (a) Sub-glacial, basaltic volcanic cone on the northern part of the Tibetan Plateau. (b) Photomicrograph of a typical Tibetan basalt showing pyroxene and plagioclase phenocrysts set in a microcrystalline groundmass (crossed polars; width of view 4 mm).

Table 3: Selected olivine analyses

Sample no.:	K98G193	K98G193
SiO_2	39·86	40·09
TiO_2	0·04	0·03
Al_2O_3	0·02	0·01
FeO	16·32	16·09
MnO	0·31	0·20
MgO	44·42	44·84
CaO	0·24	0·20
Na_2O	0·00	0·00
K_2O	0·00	0·02
Cr_2O_3	0·04	0·03
Total	101·25	101·49
Cations on basis of 4 oxygens		
Si	0·9951	0·9964
Ti	0·0008	0·0005
Al	0·0006	0·0002
Fe	0·3409	0·3347
Mn	0·0066	0·0042
Mg	1·6526	1·6609
Ca	0·0063	0·0053
Na	0·0000	0·0000
K	0·0000	0·0006
Cr	0·0007	0·0006
Sum	3·0036	3·0032

titaniferous magnetite (Table 6), and biotite is a Mg-rich phlogopite (Table 7).

The compositional data place some constraints on the petrogenesis of the lavas. The olivine phenocrysts are too Fe rich to have been in equilibrium with mantle peridotite, indicating that significant fractionation has occurred, consistent with the prominent compositional zonation of the plagioclase phenocrysts. The clinopyroxene compositions indicate temperatures between 900 and 1200°C, whereas the orthopyroxenes fit closely to the 1100°C isotherm (Fig. 3a), suggesting that magmatic temperatures were ~1100°C. Additionally, the high Al/Ti ratios of the clinopyroxenes are indicative of crystallization at medium to high pressures (mid–lower crust). In comparison, the feldspars conform only very broadly to a 1000–1100°C isotherm (Fig. 3b), indicating that some alteration or down-temperature equilibration may have occurred. The oxides are usually altered and exsolved, although one ilmenite–magnetite pair also records temperatures of ~1100°C (Table 6) and suggests that oxygen fugacities were elevated above the QFM (quartz–fayalite–magnetite) buffer ($-\log f_{O_2}$ ~8·6). Finally, the crystallization of Mg-rich biotite suggests that these were potassium-rich magmas with significant H_2O contents.

GEOCHEMISTRY AND ISOTOPE SYSTEMATICS

Major and trace element analyses were performed using standard X-ray fluorescence (XRF) and instrumental neutron activation analysis (INAA) techniques at Clermont-Ferrand (samples K89G159–200), The Open University (samples K9001–9039) or Beijing (remaining samples). Analyses for samples COUL 311, 328 and 338 are from Coulon *et al.* (1986). Sr and Nd isotope analyses on samples K9001–9039 were performed at The Open University and results from analysis of standards have been given by Turner *et al.* (1993). Sr and Nd analyses for samples K705–K738 were determined in Beijing. All of the Pb and the remaining Sr and Nd isotope analyses were performed at Clermont-Ferrand, and details of procedures and standards have been given by Arnaud *et*

Table 4: Selected pyroxene analyses

Sample no.:	K89G193	K89G193	K89G193	K89G193	K89G193	K89G194	K89G194	K89G194	K89G194	K9031	K9031	K9032	K9032	K9032
SiO_2	51·44	52·27	51·83	52·72	50·94	51·57	51·49	52·73	51·33	50·25	52·94	53·71	52·47	52·87
TiO_2	1·05	0·66	0·95	0·63	1·39	0 94	1·04	0 77	1·03	1·04	0·47	0 36	0·33	0·36
Al_2O_3	4·02	3·79	3·70	1·86	3·96	3·40	3·98	2·06	4·49	4·60	2·95	1·91	4·18	3·64
FeO	6·44	6·57	6·39	8·96	6·05	6·60	7 07	8·10	7·29	9·55	15·44	16·61	14·70	15·01
MnO	0·15	0·03	0·19	0·20	0·17	0·19	0 17	0·27	0 20	0·22	0·29	0·37	0·28	0·31
MgO	16·10	17·09	16·2	14 57	15·35	15·88	15·46	17·08	15·43	14·66	26·24	25·61	25·67	26·15
CaO	19·92	18·33	20·3	20 61	20·79	20·51	19·98	18·74	19 52	17·97	1·71	1·58	1·65	1·60
Na_2O	0·58	0·75	0·58	0·75	0 44	0 42	0·67	0·37	0·79	0·74	0·07	0·05	0 13	0·10
K_2O	0·00	0·00	0·00	0 00	0 00	0·00	0·05	0·00	0·01	0 00	0·00	0·00	0·00	0·01
Cr_2O_3	0·15	0·29	0·26	0 07	1 32	0·20	0·21	0 00	0·05	0·17	0·10	0·02	0·16	0·11
Total	99·85	99·78	100·40	100·37	100·41	99·71	100·12	100·12	100·14	99·20	100·21	100·22	99·57	100·16
Cations on basis of 6 oxygens														
Si	1·8916	1·9131	1·8973	1·9532	1·8714	1·9037	1·8951	1·9391	1·8876	1·8797	1·9125	1·9475	1·8999	1·9057
Ti	0·0290	0·0182	0·0262	0·0176	0·0384	0 0261	0·0288	0·0213	0·0285	0·0293	0·0128	0·0098	0·0090	0·0098
Al	0·1743	0·1635	0·1597	0·0812	0·1715	0·1480	0·1727	0·0893	0·1947	0·2029	0·1256	0·0816	0·1784	0·1547
Fe	0·1981	0 2012	0·1957	0 2777	0 1860	0·2038	0·2177	0·2492	0·2243	0·2989	0·4667	0·5039	0·4454	0·4527
Mn	0·0047	0·0009	0·0059	0·0063	0·0053	0·0059	0·0053	0·0084	0·0062	0·0070	0·0089	0·0114	0·0086	0·0095
Mg	0·8824	0·9322	0·8838	0·8045	0·8404	0·8737	0·8480	0·9361	0·8456	0·8173	1·4127	1·3839	1·3853	1·4048
Ca	0·7849	0·7188	0·7963	0·8182	0·8184	0·8113	0·7880	0·7384	0·7692	0·7203	0·0662	0·0614	0·0640	0·0618
Na	0·0414	0·0532	0·0412	0·0539	0·0313	0·0301	0·0478	0·0264	0·0563	0·0537	0·0049	0·0035	0 0091	0·0070
K	0·0000	0·0000	0·0000	0·0000	0·0000	0·0000	0·0023	0·0000	0·0005	0·0000	0·0000	0·0000	0·0000	0·0005
Cr	0·0044	0·0084	0·0075	0·0021	0·0383	0·0058	0·0061	0·0000	0·0015	0·0050	0·0029	0·0006	0·0046	0·0031
Sum	4·0108	4·0095	4·0136	4·0146	4·0010	4·0084	4·0119	4·0082	4·0143	4·0140	4·0131	4 0036	4·0043	4·0095

Table 5: Selected feldspar analyses

Sample no.:	K89G193	K89G193	K89G193	K89G193	K89G193	K89G193	K89G194	K89G194	K89G197	k9031	k9031	K9032	K9032	K9032
SiO_2	66·14	65 80	65·85	66·23	65·53	65·57	58·89	66·50	65 75	56·66	56·99	57·46	56·80	57·17
TiO_2	0·01	0 02	0·04	0·00	0·25	0·26	0·00	0·00	0·03	0·09	0·09	0·09	0·09	0 11
Al_2O_3	18·76	18·79	18·62	18·65	19·02	19 50	25·29	18·58	18·95	25·88	26·11	26·07	26·42	25·90
FeO	0·15	0·14	0·22	0·25	0·44	0·38	0·29	0·08	0·04	0·42	0·45	0·44	0·44	0·39
MnO	0·03	0·01	0·00	0·00	0·02	0·00	0·02	0·00	0·02	0·02	0·00	0·02	0·02	0·02
MgO	0·00	0·00	0·00	0·00	0·00	0 00	0·35	0·00	0·00	0·03	0·03	0·03	0·03	0·03
CaO	0·37	0·42	0·42	0·34	0·53	1 07	7·41	0·24	0·00	8·48	8·67	8·61	9·13	8·37
Na_2O	4·52	4·40	4·38	4·88	5·21	6 56	6 02	5·60	2·41	5·56	5·52	5·49	5·37	5·83
K_2O	10·02	10·48	10·34	9·53	8·92	6·61	1·71	8·99	13·70	1·32	1·29	1·29	1·15	1·42
Cr_2O_3	0·00	0·05	0·02	0·08	0·01	0·00	0·00	0·06	0·00	0·00	0 00	0·00	0·00	0·00
Total	100·01	100·10	99·90	99·95	99·94	99·96	99·98	100·05	100·90	98·46	99·15	99·50	99·45	99·24
Cations on basis of 32 oxygens														
Si	11·9715	11·9344	11·9598	11·9796	11·8615	11·7844	10·5780	11·9944	11·9422	10·3635	10·3516	10·3907	10·2917	10·3815
Ti	0·0011	0·0025	0·0060	0·0005	0·0345	0·0345	0·0000	0 0000	0·0041	0·0124	0·0123	0·0122	0·0123	0·0150
Al	4·0027	4·0173	3·9864	3·9766	4·0586	4·1320	5·3555	3·9509	4·0577	5·5806	5·5912	5·5579	5·6436	5·5447
Fe	0·0230	0·0211	0·0337	0·0380	0·0668	0·0578	0·0436	0·0121	0·0061	0·0643	0·0684	0·0666	0·0667	0·0593
Mn	0·0046	0·0017	0·0000	0·0000	0·0036	0 0000	0 0030	0·0000	0·0031	0·0031	0·0000	0·0031	0·0031	0·0031
Mg	0·0000	0·0000	0·0000	0·0000	0·0000	0·0000	0·0937	0·0000	0·0000	0·0082	0·0081	0·0081	0·0081	0·0081
Ca	0·0725	0·0808	0·0821	0·0659	0·1034	0·2056	1·4262	0·0464	0·0000	1·6620	1·6874	1·6683	1·7726	1·6286
Na	1·5866	1·5464	1·5424	1·7102	1·8299	2·2856	2·0966	1·9584	0·8487	1·9718	1·9441	1·9249	1·8866	2·0527
K	2·3146	2·4256	2·3965	2·1984	2 0598	1·5160	0·3919	2·0687	3·1746	0·3080	0·2989	0·2976	0·2658	0·3290
Cr	0·0000	0·0072	0·0023	0·0112	0·0010	0·0000	0·0000	0·0086	0·0000	0·0000	0·0000	0·0000	0·0000	0·0000
Sum	19·9766	20·0369	20·0093	19·9803	20·0191	20·0158	19·9885	20·0394	20·0365	19·9738	19·9620	19·9294	19·9505	20·0220

Table 6: Ilmenite–magnetite pair (sample K98G193)

	Magnetite	Ilmenite
SiO_2	0 07	0·08
TiO_2	9·79	39·39
Al_2O_3	1 93	0·34
FeO	77·87	51·30
MnO	0 20	3·42
MgO	1·44	2·86
CaO	0·03	0·08
Na_2O	0·00	0·10
K_2O	0·02	0·06
Cr_2O_3	0·07	0·00
Total	91·42	97·63
Cations on basis of 3 and 2 oxygens, respectively		
Si	0·0024	0·0015
Ti	0·2573	0·5372
Al	0·0795	0·0073
Fe	2·2768	0·7783
Mn	0·0059	0·0525
Mg	0·0750	0·0773
Ca	0·0011	0·0016
Na	0·0000	0·0035
K	0·0009	0·0014
Cr	0·0019	0·0000
Sum	2·7009	1·4605

Table 7: Selected biotite analyses

Sample no..	K89G193	K89G193	K89G193
SiO_2	44·25	42·07	43·05
TiO_2	4·15	4·92	4·60
Al_2O_3	10·64	10·81	10·77
FeO	6·46	6·34	6·74
MnO	0·08	0·08	0·05
MgO	20·28	20·40	20·88
CaO	0 02	0·03	0·01
Na_2O	0 84	0·87	0·75
K_2O	8 97	9·05	9·36
Cr_2O_3	0·00	0 03	0·05
Total	95·71	94·61	96·25
Cations on basis of 4 oxygens			
Si	6·2475	6 0438	6·0857
Ti	0·4408	0 5321	0·4890
Al	1·7714	1·8310	1·7948
Fe	0·7633	0·7621	0·7974
Mn	0·0100	0·0102	0·0065
Mg	4·2672	4·3688	4·3988
Ca	0·0025	0·0045	0·0011
Na	0·2310	0·2437	0·2058
K	1·6161	1·6591	1·6886
Cr	0·0000	0·0033	0·0052
Sum	15·3499	15·4587	15·4729

al. (1992). In light of the uncertain age of many samples and their generally young ages, no age correction was made to the isotope ratios. Only the Rb–Sr system is likely to require age corrections for Tertiary rocks but in the case of the Tibetan lavas such corrections are trivial because of their low Rb/Sr ratios. The only exception is the rhyolite sample K89G197, which has an Rb/Sr ratio of 17·8 (Table 8), and the initial $^{87}Sr/^{86}Sr$ ratio for this sample, when corrected to 6·4 Ma (Table 1), is 0·709015 (measured $^{87}Sr/^{86}Sr = 0·713700$, Table 9).

The geochemical data presented in Table 8 show that all of the samples are potassium rich. On a conventional Harker diagram of K_2O vs SiO_2 (Fig. 4a) the samples define a scattered trend between 45 and 75% SiO_2 at high K_2O (generally >3·5%), and lie almost totally within the shoshonite field as defined by Peccerillo & Talyor (1976). Despite their high K_2O, however, they are not ultra-potassic, having K_2O/Na_2O ratios between 0·5 and 2·0 (Fig. 4b), again within the field of shoshonitic magmas. The *mg*-number $[= MgO/(MgO \times 0·8 + FeO_{tot})]$ ranges from 73 to 10, and SiO_2 and Al_2O_3 increase, whereas CaO and Fe_2O_3 (which has an inflection at 5% MgO) decrease, with decreasing MgO (Fig. 5). TiO_2 (not plotted) shows an inflected trend and the absolute abundances of Al_2O_3 and TiO_2 are low, with averages of 13–15% and 1·5–2%, respectively. K_2O and Na_2O have relatively constant abundances though K_2O is always slightly greater than Na_2O ($K_2O/Na_2O \leqslant 2$). The rhyolites broadly lie at the projected end of the trends defined by the more mafic compositions, being highly depleted in TiO_2, MgO and CaO, whereas K_2O and Na_2O abundances remain similar to those of the mafic lavas.

Those trace elements that are compatible in olivine and clinopyroxene, such as Ni, Cr and Sc, all decrease rapidly with MgO (Fig. 6), the more mafic lavas having high abundances (140 p.p.m. Ni, 500 p.p.m. Cr). Falling off this trend are the Ulugh Muztagh rhyolites and some of the rhyolites from the Shiquanhe area, which have fairly high Ni (Fig. 6). Plagioclase is a major phenocryst phase and, although the absolute abundances of Sr are very

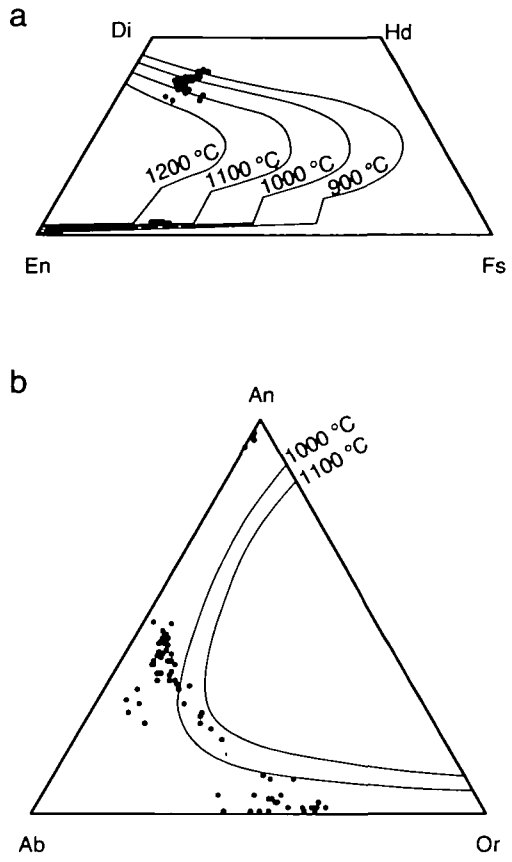

Fig. 3. Phenocryst composition data from selected mafic lavas suggest crystallization from relatively primitive magmas at temperatures in excess of 1000°C. (a) Pyroxene quadrilateral with method of projection and 5 kbar temperature contours from Lindsley (1983). (b) Feldspar ternary diagram with 5 kbar temperature contours from Fuhrman & Lindsley (1988).

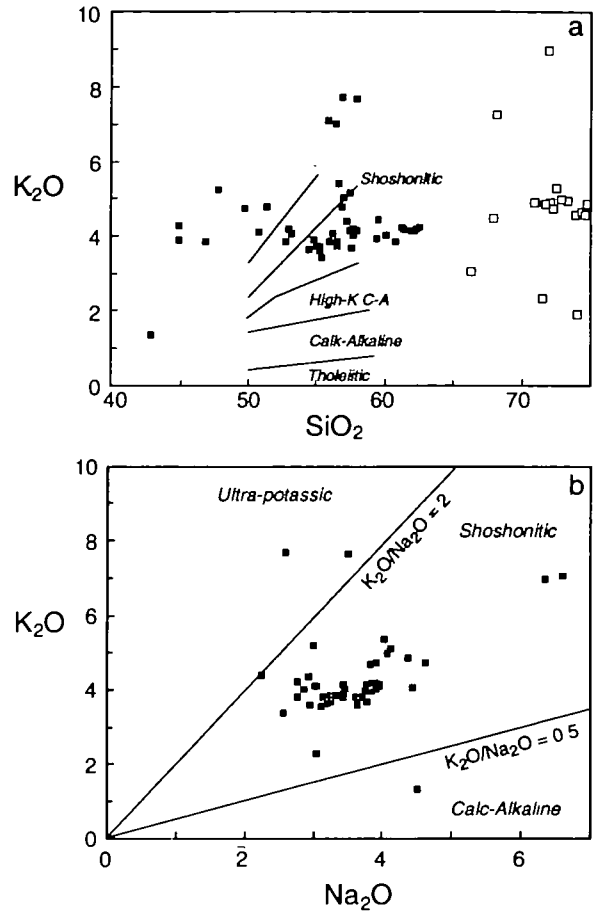

Fig. 4. Tibetan lavas plotted on (a) a K_2O vs SiO_2 and (b) a K_2O vs Na_2O diagram, showing that they are shoshonitic rather than calc-alkaline or ultra-potassic in character. For the vast majority of the mafic lavas, K_2O remains relatively constant (3·5–4·5%) over a wide range of SiO_2 and Na_2O, suggesting buffering by a residual phase in the source region, most probably phlogopite. The rhyolites, which are shown as open squares in (a), are not plotted in (b).

high, typically 600–4800 p.p.m. in the mafic lavas, Sr also shows a positive correlation with MgO (Fig. 6). The rare earth patterns for the mafic lavas do not show negative Eu anomalies consistent with moderately elevated f_{O_2} (Fig. 7).

A characteristic feature of the Tibetan lavas is their extreme enrichment in all of the incompatible elements (Table 8). For example, La contents range from >110 to 540 p.p.m. in the mafic to intermediate rocks, making these among the highest abundances reported from igneous rocks. Moreover, some of the highest concentrations are found in the more primitive samples (Fig. 6). In general, however, there is only a weak correlation between incompatible element abundance and indices of differentiation such as MgO, and most plots show considerable scatter (Fig. 6). Primitive mantle-normalized incompatible element diagrams illustrate the enriched nature of the Tibetan lavas (Fig. 7). Abundances range from several times primitive mantle for Y and the HREE, to several hundred times for Rb, Ba and Th, with steep rare earth element (REE) patterns and high LREE/HREE ratio. Significant departures from the overall pattern are negative anomalies for Sr, Nb, Ta and K which occur despite their overall very high abundances (see Fig. 7 and Table 8). Negative Ti anomalies are ubiquitous and some samples also have small negative Ba and Zr anomalies (Fig. 7). The mafic lavas may be broadly divided into those with higher Rb/Ba (Fig. 7a) and those with lower Rb/Ba (Fig. 7b).

All of the available samples have been analysed for Sr, Nd and Pb isotopes (Table 9). The results show a relatively broad range of high $^{87}Sr/^{86}Sr$ (0·7076–0·7106) at more restricted ε_{Nd} (−5·2 to −8·1) forming a cluster well displaced into the enriched

Table 8: Major and trace element analyses of Tibetan lavas

Sample no.:	K89G185	K89G186	K89G191	K89G192	K89G193	K89G197	K89G200	Kp 24-1	k705	k708	k713	k716	k718	k720	k723	K732	K738	KP12-5B	Bg 121	Bg 124	Kp 35-10	Kp39-3
Location:	I	I	I	I	I	I	I	III	IV	IV	IV	IV	IV	IV	IV	IV	IV	IV	VI	VI	VII	VII
SiO_2	51·42	49 80	56·95	57 50	57·09	75 10	56·67	56 56	52·79	57·28	55·09	57 62	57·98	55·34	55·25	56·22	55·44	59 56	60 80	57·60	54 88	47·85
TiO_2	1 85	1·77	1·36	1·32	1·31	0 10	1·43	1·90	1 87	1·85	2 27	2 23	2·12	2·23	2·23	2·28	2·32	1·75	1 50	1·26	1·88	1·89
Al_2O_3	14 62	13·65	14·10	14·15	14·31	12·95	13·80	14·49	13·49	14 12	14·42	14 11	14·04	14 10	14·21	14·54	14·12	14 24	15·20	14·20	15·55	12·32
$Fe_2O_3^*$	9·61	9 11	7·34	6·89	7·07	0·95	7·31	7·99	8 34	8·17	8·03	8·12	9·33	8 76	8·92	8 78	11·04	8 14	8·00	6·31	6 44	9·14
MnO	0·14	0·12	0 10	0·09	0·09	0·01	0 10	0·11	0·10	0 10	0 11	0·12	0 11	0·13	0·15	0·11	0·14	0·10	0·08	0·09	0·13	0·13
MgO	4·03	5 60	3·80	3 36	3·67	0 04	4·37	3 85	3·74	2·92	3·02	2 80	2·65	3·84	3·75	2 90	3·67	2·23	2 76	2·82	2·52	7·86
CaO	7·59	7·20	6·45	5 85	6·74	0 60	6·35	5 60	7·15	5·36	6·28	5 25	5·07	6·32	6 35	5·14	6·33	4·43	4·94	7·28	4·90	7 87
Na_2O	4 60	3·80	3 89	4·10	4·06	4·35	4·02	2·92	2·76	2 91	3·24	3 04	3 01	2·93	3 11	2·84	2·56	3·49	3·41	3·18	3·23	2·98
K_2O	4·77	4 70	4 75	5·15	4 99	4·90	5 40	4·31	3·83	4 37	3 69	4·14	4·12	3·62	3 57	4·04	3·39	4·33	3·85	3·68	3·88	5·22
P_2O_5								1·07	1·04	0·92	1·11	1·16	1 13	1·14	1·16	1·23	1 12	1·00	0·66	0·65	0·86	1·29
LOI	2 09	4·15	1·01	1 15	1 04	0 50	0·32	0 39	5·11	2·06	2·62	1 56	0·91	1·77	1 78	1·46	1·10	1·05	0·97	1·89	2·65	3 16
Total	100·72	99·90	99·75	99·56	100 37	99·50	99·77	99·19	100·22	100·06	99·88	100 14	100·47	100 18	100·48	99·54	101·23	100 32	102·17	98·96	96·92	99·71
mg-no.	0·49	0 59	0 55	0·53	0·55	0·09	0 58	0·53	0·51	0·45	0·47	0·45	0 40	0·51	0·49	0·44	0·44	1·00	0·45	0·51	0·48	0·67
Sr	2011	1756	1410	1397	1368	64	1567	1158	1250				944			1101	914		1150	1096	968	1841
Ba	2563	2564	2080	2091	1760	86	2076									1985	2206					
Rb	122	178	120	188	193	1139	198	136	118				175			137	109		122	130	107	166
Ta	1·6				2 3		1·5												1·7	1·4		1·8
Th	27	24	48	49	50	66	44									27	33		36	36		16
Hf	8	9	7	10	8	8	10												11	10		12
Zr	412	358	230	318	368	27	407	488								461	550		552	516	414	516
Sc	10	13	13	12	8	3	9									12	14		8	8		20
Ni	72	64	70	59	58	0	61	55								51	45		35	33	37	100
Cr	88	122	137	109	81	9	83	89								239	73		65	61	76	258
V		127	95	97		3		61								121	133		88	75	99	222
Nb	31				36		26									38	44					
Y	32	17	21	24	23	9	23		13	16	18	17	18	18	18	28	32					
Pb	29	30	27	35	27	19	35									34	42					
U	3					98	7									2	3					
Ga	22	17	20	21	22	29										16	20					
La	177	183	137	156	151	79	161	202	154	140	146	154	162	154	170	170	148	180	162	138	134	111
Ce	333	358	263	290	274	103	287	388	260	234	230	260	300	280	300	326	260	320	319	275	260	229
Pr		37	27	29		7		40										34			26	
Nd	142	141	96	105	106	15	119	146	120	104	100	116	126	120	132	154	129	112	117	101	98	101
Sm	20·2	20·0	13·0	15·0	13·6	1·7	16·1	21 2	11·6	12·3	14·7	14·0	14·2	13·0	13·3	21 6	19·2	16 0	13·8	12·3	14 6	17·1
Eu	4·3	4·7	3·0	3 2	3·0	0 2	3·6	4 1	2·8	2·7	3·4	3 2	3·0	2·9	3·0	3·2	2 6	2·9	3·4	2 8	3·3	4 1
Gd		12·0	8·3	9·2		1·0		15·1	5 8	6·6	8·0	7·4	7·8	7 2	7·3	8 3	6·4	8 3			10·9	
Dy		6·3	4 5	4·9		1·0		5·7	3·1	3·6	4·6	3·7	4 2	4 2	4·1	4·4	3·8	4·1			6·2	
Er		2·7	2·1	2 4		1 0			1·4	1·5	1·8	1·6	1·8	1·9	1·9	2·0	1·7	1·7				
Tb	1·3				0·9		1·0	2·1										1·0			1 5	1·4
Yb	1·5	1·5	1·6	1·8	1 6	1·3	1·4	2·4	0 8	1·1	1·3	1·1	1 1	1·3	1·3	1·3	1·2	1·3	1·4	1·4	3·2	1 8
Lu	0·2	0 2	0 2	0·3	0 2	0·2	0·2	0·9										0 2	0·2	0·1	0 6	0·3

(continued on next page)

Table 8: continued

Sample no.:	Kp47-2	Kp47-5	Kp23-2	Bb-88	Bb-89	Bb-95	Bb-105	Bb-107	Bb-109	Bb-114	Bb 94-2	K9006	K9007	K9008	K9016	K9018	K9021	K9026	K9028	K9031	K9032	K9038
Location:	VII	VII	VII	VIII	VIII	VIII	VIII	VIII	VIII	VIII	VIII	VIII	VIII	VIII	VIII	VIII	VIII	VIII	VIII	VIII	VIII	VIII
SiO_2	50·81	52·97	53·27	44·90	46·90	56·90	55·90	44·90	56·40	42 90	58 00	62 23	59·44	61 34	62 53	61 47	62·02	57·71	54·51	55·95	57·69	55·31
TiO_2	1·55	1·57	2 34	1·30	1·95	0·93	0·41	1 24	0·35	1·72	0 56	1·60	1·54	1 62	1 47	1·59	1·57	1·69	1 53	1·55	1·63	1·59
Al_2O_3	14·03	13·89	15·77	12·42	13·40	17·40	19·10	12·40	18 21	12·60	19·50	15·24	15·30	15·15	15·05	15·09	15·14	15 95	14·94	15·19	15·76	15·83
Fe_2O_3*	7·32	8·66	9·41	14·78	9·56	7·42	5·00	9·91	4·60	9 85	4·31	6 03	6·13	6·22	5 69	6 13	5·92	6·80	6 33	6·86	7·20	5·88
MnO	0·09	0 12	0·13	0 16	0·16	0 09	0 16	0·16	15 00	0·17	0·07	0 08	0·09	0·09	0·08	0 08	0 08	0·09	0·09	0·10	0·10	0·15
MgO	3 95	4·23	4·20	8·05	7·09	1·64	0·44	10 30	0·44	6·25	0 80	1·75	1·87	1 23	1 59	1·76	1·77	2·79	2 75	3·35	2·88	2·53
CaO	9·53	7·21	6·00	11·37	11·46	3·38	2·60	12 10	2·10	9·47	2·12	3·97	4·75	3·77	4·20	4·32	3·99	5 45	7·64	6·30	5 04	7·38
Na_2O	4·42	3·43	3·44	2·75	3·13	2·58	6·60	3·31	6·34	4·50	3·48	3 88	3 42	3·82	3·87	3 77	3·77	3·95	3·62	3·61	3·82	3·63
K_2O	4·09	4 18	4·06	4·25	3·82	7·71	7 08	3·89	7·01	1 35	7·68	4·14	3 93	4 21	4·21	4·15	4·12	4·17	3·62	3·83	4·01	3·71
P_2O_5	1·02	0·91	1·20	0·18	1·50	0·83	0·06	1·53	0 06	1·50	0·11	0·86	0·78	0·84	0 79	0·85	0 84	0·84	0·76	0 82	0·84	0·83
LOI	2·21	2·58	1·00	1·06	2·48	1·98	2·34	1·91	3·36	9·55	1·98	1 08	2·97	0·94	0·78	0·99	0·81	0·89	3·80	1·99	0·90	3·26
Total	99·0	99·75	100·82	101·22	101·45	100·86	99·69	101·65	113·87	99·86	98·61	100 86	100·22	99·23	100·26	100 20	100·03	100·33	99·69	99·65	99·87	99·90
mg-no	0·56	0·53	0·51	0·56	0·63	0·34	0·17	0 71	0·18	0·60	0 30	0·40	0·42	0 32	0·39	0·40	0·41	0·49	0·50	0·53	0·48	0·50
Sr	1621	1562	1279	4810	4735	4040	2306	2941	1700	3214	2295	700	686	713	635	713	686	1019	987	983	1040	1075
Ba			105									1454	1387	1466	1267	1398	1389	1611	1527	1626	1814	1315
Rb	103	144		217	75	217	314	213	348	136	290	212	198	214	243	208	211	123	109	119	122	98
Ta	2 3	1·5		4 9	2·5	1·8	1·9	1·3	5·1	1·9	2·6		2·5	2 6			2·5		2 2	2·2		2·2
Th	9	18		67	80	114	216	89	267	76	145	32	31	33	34	31	32	23	21	22	23	9
Hf	9	9		9	13	13	27	9	31	8	23		11	11			11		9	9		7
Zr	348	399		985	695	587	1828	443		509	1360	509	504	507	469	501	514	450	411	433	445	328
Sc	19	16		23	18	8	1	23	1	20	2	8	8	7	8	12	10	11	13	14	11	15
Ni	60	87	37		90	37	4	148		109	10	16	21	21	11	20	21	30	33	39	46	55
Cr	125	79	38		220	70	3	520	112	360	13	18	15	21	40	16	15	35	43	62	83	109
V	162	169	85		263	63	63	186		186	66	98	92	96	83	95	96	117	105	116	124	133
Nb												40	39	39	37	39	39	40	37	39	39	36
Y												26	28	26	25	27	27	26	25	25	28	25
Pb												39	67	29	27	36	39	27	25	30	30	21
U												5	5	5	8	6	6	2	1	3		
Ga												21	22	22	23	22	23	20	18	18	21	20
La	154	165	184	471	382	328	390	326	542	217	334		136	133			137		112	116		82
Ce	288	304	352	706	724	572	577	658	685	412	530		255	255			258		212	224		163
Pr			36																			
Nd	108	114	130	341	262	204	137	250	198	156	146		98	98			96		81	87		68
Sm	17·3	19·4	19·6	44·1	36 4	26·0	17·3	33 4	16·7	21·5	18·9		13·6	13·4			13·1		11·4	11·8		9·8
Eu	3·7	4·4	4·2	10 2	9·1	6·6	3 9	8·4	4·3	5 6	4·5		2·9	2·9			2·9		2 7	2 8		2·6
Gd			13 9																			
Dy			6·9																			
Er			2·4																			
Tb	1·4	1·5	2·0	2·6		1·9		2·5	1·7		1·7		1·1	1 1			1 1		1·0	1·0		0·9
Yb	2·0	1·9	2·7	2·5	3·0	2·5	5·1	2·3	5·3	2·1	3·6		2 1	2·0			2·1		1·8	1·8		1·9
Lu	0·3	0·3	0·8	0·4	0 5	0·3	0 5	0 3	0 7	0·3	0 5		0·3	0·3			0·3		0·3	0·3		0·3

Sample no.	K9039	K9024	K9027	K9029	K9002	K9017	K9019	COUL 311	COUL 326	COUL 328	COUL 338	COUL 339	K89G159	K89G162	K89G163
Location:	VIII	IX	V-IX	V-IX	V-IX	V-IX	V-IX	XI	XI	XI	XI	XI	X	X	X
SiO_2	56·57	56·57	57·49	56·26	71·48	62·36	60·16	73·93	67·96	63·03	52·07	52·67	68·19	63 78	64·85
TiO_2	1·71	1·58	1·68	1·63	0·63	1·56	1·63	0·27	0·46	0·59	1·02	1·05	0·74	0·81	0·77
Al_2O_3	16·25	15·41	15·96	15·60	13 79	15 26	14·95	13 78	15·97	16 44	18·19	18·89	14·01	14·30	14·04
Fe_2O_3*	7·48	7·05	6·82	6·68	4·28	5·97	6·23	2 07	2·78	4·16	8·06	8 44	2·88	3·39	3 41
MnO	0·04	0·10	0 09	0·09	0·07	0·07	0 09	0·05	0·03	0·06	0·16	0·17	0·02	0·05	0·06
MgO	1·22	3·21	2·88	2·78	1·50	1·66	1·83	0 37	0 96	1·90	3·58	3·84	1·01	2·26	1 87
CaO	5 74	5·64	5·39	6·28	1·80	4·04	4·65	1·26	2·66	4·15	8·90	8·00	1 33	2·88	2·93
Na_2O	3·75	3·69	3·95	3·90	3·04	3 76	3 73	2·67	4·10	4·25	3·04	3·39	3·15	2·99	3·30
K_2O	3 71	3·81	4·11	4·06	2·30	4·15	4·01	4·56	4 47	3·47	1 98	1·21	7·25	7·22	6·43
P_2O_5	0 87	0·91	0·85	0·76	0·14	0·85	0·88	0·02	0·16	0·29	0·26	0·27			
LOI	2 27	1·82	0·79	1·87	1·81	0·85	1·90	1·41	0·62	1·05	1·33	1·41	0·53	2·10	1·75
Total	99·61	99·79	100·01	99·91	100·84	100·53	100·06	100 39	100·17	99 39	98·59	99·34	99 11	99·78	99·41
mg-no.	0·28	0 51	0·50	0·49	0 45	0 39	0·41	0·29	0·45	0·52	0·51	0·51	0·45	0·61	0·56
Sr	1092	1025	1029	1014	196	712	747	119	752	893	772	770	984	976	816
Ba	1479	1635	1631	1595	407	1413	1452						2131	2211	1860
Rb	94	118	121	123	99	217	189	184	174	142	56	33	495	515	471
Ta		2·4	2·3										1·4	1·6	1·4
Th	13	23	23	21	9	32	30						107	115	106
Hf		9	10										12	13	12
Zr	338	433	452	436	215	499	495	187	149	141	122	115	422	426	400
Sc	14	15	12	13	9	10	9						4	7	6
Ni	63	51	32	33	34	20	23	0	9	5	22	19	0	37	33
Cr	107	86	47	35	76	18	21	9	23	26	53	37	59	59	59
V	140	117	117	107	72	92	94	11	54	87	199	227			
Nb	39	39	40	41	11	40	39	14	6	6	6	5	21	22	23
Y	27	26	27	24	24	26	26						15	16	14
Pb	22	32	35	29	12	45	38						114	102	107
U		3	1	3	1	5	4						8	8	11
Ga	21	19	20	20	15	22	21						19	19	21
La		122	123					36	28	33	18	15	83	85	86
Ce		233	232					72	56	68	38	33	177	204	181
Pr								7	5	7	4	3			
Nd		90	90					26	22	28	18	16	87	101	87
Sm		12·3	12·2					5 3	3·7	5·1	4 3	3·8	12·7	15·6	12·7
Eu		2·9	2·9					0·7	0 9	1·2	1·3	1·3	2·3	2·9	2·4
Gd								4 4	2·3	3·3	4 2	4·0			
Dy								4 3	1·3	2·0	3 5	3·6			
Er								2 8	0·6	1·0	1·8	2 0			
Tb		1·0	1·0										0·7	0·7	0·6
Yb		1·9	2·0					3·0	0·6	0 9	1·0	1·6	1·2	1·0	1·1
Lu		0·3	0 3					0·5	0·1	0·1	0·1	0·2	0·1	0·2	

Table 9: Sr, Nd and Pb isotopic data from Tibetan lavas

Sample no.	Location	$^{87}Sr/^{86}Sr$	$^{143}Nd/^{144}Nd$	ε_{Nd}	TDM*	TDM source†	$^{206}Pb/^{204}Pb$	$^{207}Pb/^{204}Pb$	$^{208}Pb/^{204}Pb$	Pb model age	$\mu 1$	$\mu 2$
K89G185	I	0·708070	0·512330	−6·01	0·91	1·14	18·714	15·691	39·120	3·1	8·05	12·20
K89G186	I	0·708050	0·512370	−5·23	0·87	1·08	18·680	15·656	39·015	3·0	7·99	12·27
K89G191	I	0·708150	0·512340	−5·81	0·87	1·07	18·719	15·677	39·028	3·1	8·02	12·33
K89G192	I	0·708120	0·512360	−5·42	0·88	1·10	18·739	15·705	39·115	3·2	8·07	12·24
K89G193	I	0·708120	0·512330	−6·01	0·86	1·03	18·756	15·708	39·116	3·2	8·07	12·31
K89G197	I	0·713700	0·512350	−5·62	0·78	0·90	18·887	15·674	39·013	2·8		
K89G200	I	0·708170	0·512310	−6·40	0·91	1·11	18·747	15·718	39·304	3·2	8 09	12·19
Kp 23-1	II	0·708690	0·512315	−6 30			18·727	15·662	38·917	2·9	7·99	12·48
Kp 23-3	II	0·708690	0·512329	−6·03			18·736	15·671	38·900	3·0	8 01	12·47
Kp 24-1	III	0·710340	0·512263	−7·32	1·01	1·27	18·834	15·689	39·190	3·0	8·03	12·87
kp12-2	IV	0·709327	0·512277	−7·04								
kp12-5	IV	0·709842	0·512253	−7·51								
Kp 12-7	IV	0·707570	0·512340	−5·81			18·711	15·668	38·997	3·0	8·01	12·35
k705	IV	0·710373	0·512265	−7·28	0·82	0·92						
k708	IV	0·710230	0·512277	−7·04	0·88	1·03						
k713	IV	0·710376	0·512259	−7·39	1·02	1·29						
k716	IV	0·709911	0·512282	−6·94	0·88	1·04						
k718	IV	0·709875	0·512264	−7·30	0·87	1·01						
k720	IV	0·709832	0·512272	−7·14	0·85	0·98						
k723	IV	0·709960	0·512291	−6·77	0·81	0·91						
k731	IV	0·710540	0·512221	−8·13								
K732	IV	0·710540	0·512221	−8·13	1·03	1·28						
K738	IV	0·710051	0·512365	−5·33	0·90	1·15						
Kp 12-4	IV	0·709170	0·512261	−7·35			18·714	15·673	39·987	3·0	8·02	12·33
kp10-3	V	0·708960	0·512248	−7·60			18·722	15·701	39·079	3·2	8·06	12·18
kp10-6	V	0·707920	0·512323	−6·14			18·660	15·692	39·105	3·2	8·06	11·90

Bg 121	VI	0 708670	0·512326	–6·09	0·83	0·97	18·718	15·691	39 086	3·1	8 05	12·23
Bg 124	VI	0·708770	0·512293	–6·73	0·88	1·04	18·704	15·669	39·030	3·0	8 01	12·31
Kp 35-10	VII	0 708490	0·512371	–5·21	0 89	1·13	18·718	15 687	39·131	3·1	8·04	12·25
Bb 94-2	VIII	0·708230	0·512318	–6·24	0·88	1·06	18·728	15·725	39·296	3·3	8·11	12·04
Bb 104	VIII	0·707980	0·512331	–5·99			18·739	15·713	39·282	3·2	8·08	12·18
K9006	VII	0·708248	0·512251	–7·55								
K9007	VII	0 709175	0·512292	–6·75	0·94	1·17	18·742	15·687	39·168	3·1	8·04	12·39
K9008	VII	0·709103	0·512265	–7·28	0·97	1·19	18·770	15·713	39·260	3·1	8·08	12·35
K9016	VII	0·709229	0·512243	–7·71			18·776	15·709	39·217	3·1	8·07	12·41
K9018	VII	0·709068	0·512292	–6·75								
K9021	VII	0·709155	0·512308	–6·44	0·92	1·13	18 769	15·706	39·324	3·1	8·07	12·40
K9026	VII		0·512334	–5·93								
K9028	VII	0·708198	0·512337	–5·87	0·90	1·12						
K9031	VII	0·709158	0·512333	–5·95	0·89	1·09	18·742	15·694	39·178	3·1	8·05	12·33
K9032	VII		0·512338	–5·85			18·712	15·692	39·135	3·1	8·05	12·19
K9038	VII	0·708026	0·512294	–6·71	0·96	1·21	18·675	15·679	39·001	3·1	8·03	12·08
K9024	IX	0·708374	0·512324	–6·13	0·90	1·10	18·714	15·689	39·140	3·1	8·04	12·22
K9027	V–IX	0·708189	0·512333	–5·95	0·88	1·08						
K9001	VII	0·708300	0·512224	–8·08								
K9041	VII	0·716102	0·512366	–5·31								
COUL 311	XI	0·707970	0 512650	0·23	0·75	1·25	18·672	15·607	38·912	2 7		
COUL 326	XI	0·705900	0·512480	–3·08	0·85	1·17	18·488	15 655	38·857	3·2		
COUL 328	XI	0·706410	0 512470	–3 28	0·92	1·34	18·526	15·676	38·979	3·3	8·05	11·28
COUL 338	XI	0·704930	0 512700	1 21	0 84	2·00	18·610	15·608	38·761	2·8	7·92	12 23
COUL 339	XI	0·704800	0·512710	1·40	0 85	2 12	18 591	15·592	38·730	2 7	7·89	12 24
K89G159	X	0·714810	0·512070	–11·08	1·24	1·56	18·693	15·781	39·609	3·5		
K89G162	X	0·715520	0·512030	–11·86	1·34	1·74	18·721	15·769	39·699	3·5	8·19	11·68
K89G163	X		0·512040	–11·67	1·28	1·61						

*Nd depleted mantle model age based on measured Sm/Nd.
†Nd depleted mantle model age assuming a 30% decrease of Sm/Nd during melting.

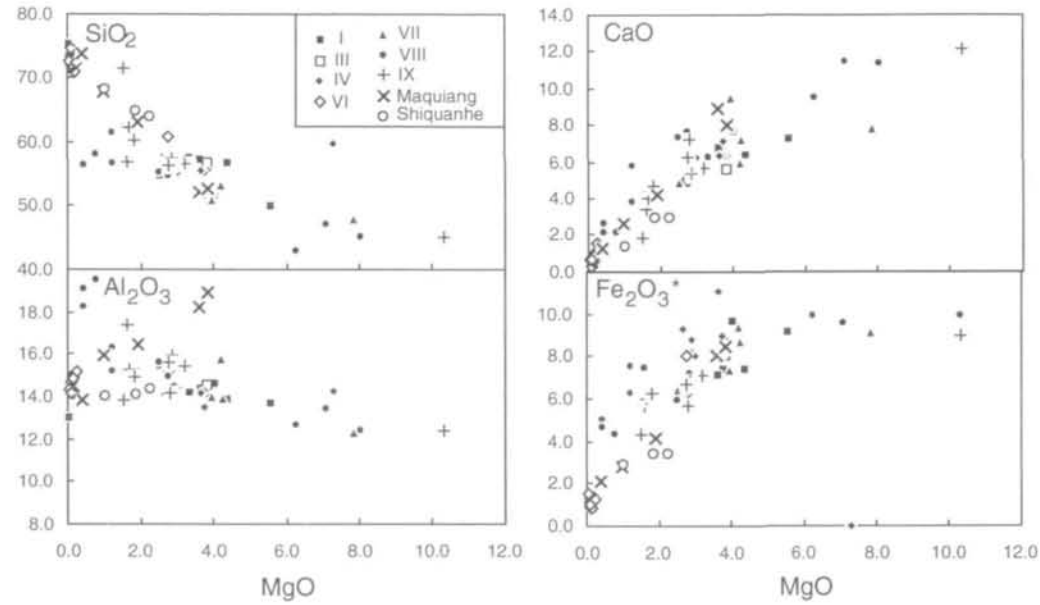

Fig. 5. Selected major element–MgO variation diagrams illustrating the broad compositional range of the Tibetan lavas which extends back to fairly magnesian compositions (MgO 8–10%). Symbols refer to sub-area in Fig. 1, as indicated in the legend.

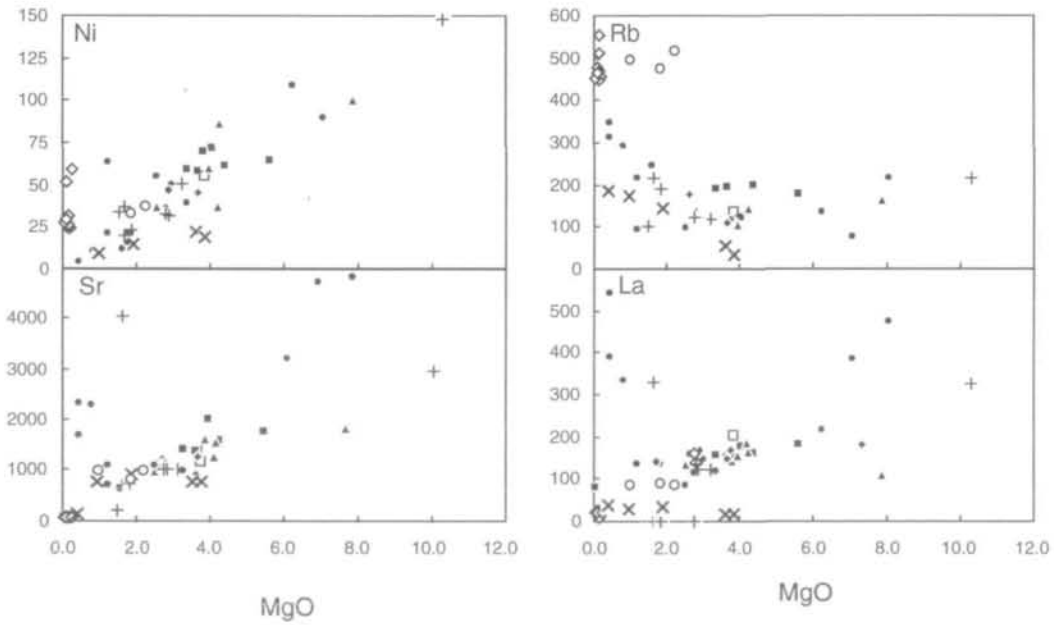

Fig. 6. Selected trace element–MgO variation diagrams which have discernible trends about which there is considerable scatter, particularly in the case of the silicic lavas. Symbols as in Fig. 5.

quadrant relative to bulk Earth (Fig. 8). Nd depleted mantle model ages are much older than the age of the lavas and show a relatively restricted range between 0·8 and 1 Ga (Table 9). Pb isotopes are characterized by a range of $^{207}Pb/^{204}Pb$ (15·51–15·72) and $^{208}Pb/^{204}Pb$ (38·67–39·30) at relatively invariant $^{206}Pb/^{204}Pb$ (18·39–18·83), leading to near-vertical arrays (Fig. 9) that lie above the northern hemisphere reference line (NHRL), well to the right of the geochron. These are unlikely to reflect crustal contamination, as sediments tend to show a broad range in $^{206}Pb/^{204}Pb$, and this is particularly true of analyses of sediments scattered along the Kunlun Range in Tibet (N. O. Arnaud, unpublished data, 1994).

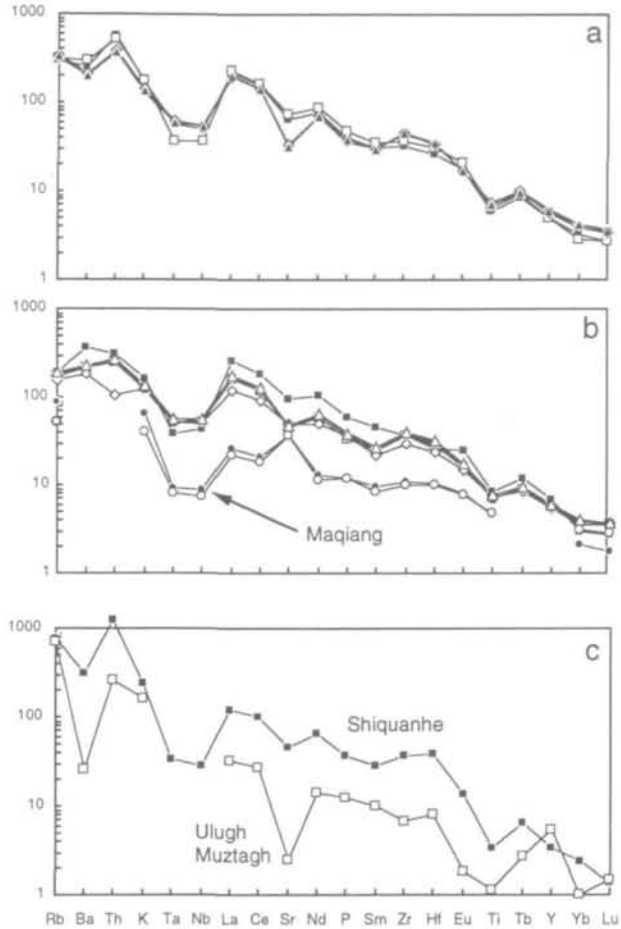

Fig. 7. Primitive mantle-normalized incompatible element diagrams for the Tibetan lavas, all of which show extreme incompatible element and LREE/HREE enrichment and have negative K, Ta, Nb and Ti anomalies. The mafic lavas can be sub-divided into those in (a), which have high Rb/Ba, and those in (b), which have low Rb/Ba. The available data from the Maquiang lavas are shown in (b). The patterns for two of the rhyolites are shown in (c) [Ta is not plotted for the Ulugh Muztagh rhyolites because the values given by McKenna & Walker (1990) almost certainly reflect contamination from milling in a tungsten carbide shatterbox]. Where trace element analyses were incomplete specific element abundances were calculated using the relationships Zr = Hf × 37·5, Nb = Ta × 16, P = Sm/15·5. Normalization factors from Sun & McDonough (1989).

Inspection of Tables 8 and 9 and Figs 5, 6, 8 and 9 shows that the rocks from the different northern subareas cannot be distinguished on the basis of the geochemical or isotopic data. In contrast, the mafic lavas described from the Maquiang area (XI) in the southern part of the plateau by Coulon *et al.* (1986) show some important differences from the northern lavas just described. These lavas have higher Al_2O_3 and lower K_2O (Table 8) and much lower abundances of incompatible elements and lower LREE/HREE ratios, although apart from their positive Sr

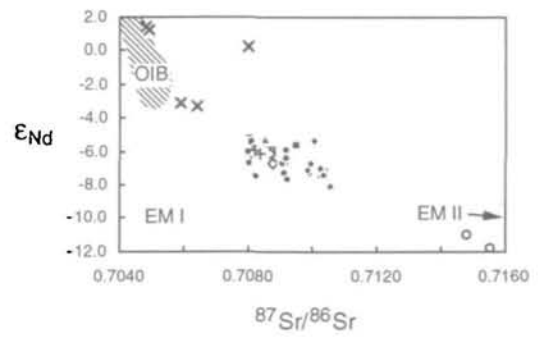

Fig. 8. Present-day ε_{Nd} and $^{87}Sr/^{86}Sr$ of the Tibetan lavas, showing their relatively broad and evolved range of $^{87}Sr/^{86}Sr$ at more restricted ε_{Nd} and indicating that the source of these lavas must have been enriched and isolated from mantle convection for a long period to develop these distinct isotopic values (the Nd depleted mantle models ages are ~0·9 Ga). The lavas from the southern parts of the plateau have strikingly more primitive $^{87}Sr/^{86}Sr$ and ε_{Nd} whereas the rhyolites have more evolved compositions. It should be noted that the Tibetan lavas do not coincide with the OIB end-members EM I and EM II proposed by Zindler & Hart (1986); symbols as in Fig. 5.

anomalies, the general shape of their incompatible element patterns is similar, with negative Nb, Ta and Ti anomalies (Table 8, Fig. 7b). They also exhibit more primitive Sr and Nd isotopic composi-

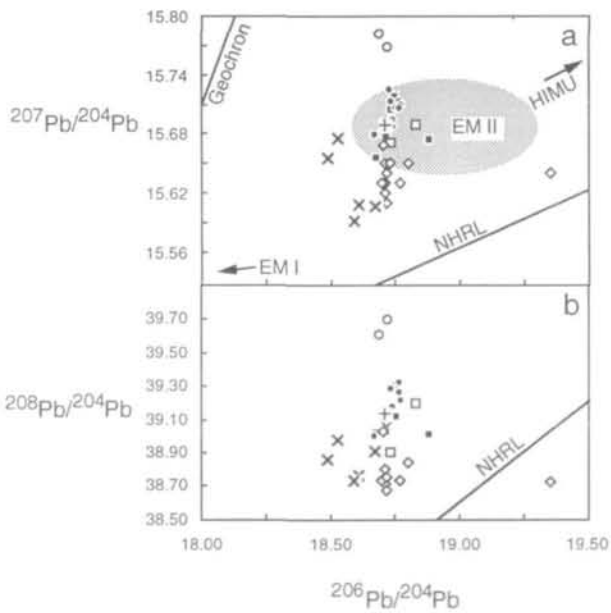

Fig. 9. Pb isotope data from the Tibetan lavas characterized by a range of $^{207}Pb/^{204}Pb$ and $^{208}Pb/^{204}Pb$ at very uniform $^{206}Pb/^{204}Pb$, leading to vertical arrays displaced well to the right of the geochron and above the northern hemisphere reference line (NHRL). The Tibetan lavas do not coincide with the OIB end-members proposed by Zindler & Hart (1986) and although they partially overlap with EM II on this diagram, comparison with Fig. 8 shows that this is not the case for Sr and Nd isotopes. Symbols as in Fig. 5.

tions ($^{87}Sr/^{86}Sr = 0{\cdot}7048$–$0{\cdot}7064$; $\varepsilon_{Nd} = 1{\cdot}4$ to $-3{\cdot}3$), and lower $^{206}Pb/^{204}Pb$ (18·53–18·61), $^{207}Pb/^{204}Pb$ (15·59–15·68) and $^{208}Pb/^{204}Pb$ (38·73–38·98).

Finally, the rhyolitic lavas (herein used to refer to lavas with >63% SiO_2) may be conveniently divided into two groups: those which have incompatible element abundances and isotopic ratios similar to the mafic lavas, and those which have much lower abundances and very high Rb/Ba ratios (Table 8, Fig. 7c). The first group include those of the Shiquanhe area sampled by Arnaud (1992), and two rhyolitic samples from the Maquiang area. The second group are exemplified by the Ulugh Muztagh rhyolites, which have been described in detail by McKenna & Walker (1990). Most of the rhyolites, particularly those with SiO_2 >70%, have isotopic compositions ($^{87}Sr/^{86}Sr$ ~0·715; ε_{Nd} ~−11; $^{206}Pb/^{204}Pb$ ~18·7; $^{207}Pb/^{204}Pb$ ~15·7 and $^{208}Pb/^{204}Pb$ ~39·7) which are consistent with the interpretation by McKenna & Walker (1990) that they represent the products of crustal melting. Some, however, have isotope ratios similar to the mafic lavas (e.g. COUL 311, Table 9), more in keeping with a fractionation origin. The petrogenesis of the rhyolitic volcanics will not be considered further here, and the reader is referred to McKenna & Walker (1990) for details about the anatectic rhyolites, which represent a crustal isotopic end-member for the petrogenesis of the remaining, mafic, more dominant volcanics.

PETROGENETIC CONSTRAINTS

Given the area of the Tibetan plateau from which the volcanic rocks have been collected, the available data preclude detailed petrogenetic modelling. Instead, the extreme compositions of the lavas can be used to place constraints on possible petrogenetic models, as their broad similarities (e.g. Figs 7a and 7b) imply a common origin. Concentrating on the mafic lavas as indicative of primary melts, they span a broad range from relatively primitive to highly evolved compositions (MgO 10–2%), and the major element trends in Fig. 5 probably reflect the effects of both partial melting and fractionation. High values of both Na and K imply derivation by small degrees of melting and additionally the high K_2O may require the presence of a potassic phase in the source. The majority of the Tibetan rocks analysed here have high K_2O, with $K_2O/Na_2O > 1$, and are therefore shoshonitic. K_2O is high regardless of the SiO_2 content of the rock (45–60%, Fig. 4) and this must reflect control by a potassic phase not only during fractionation but probably also in the mantle source region. Meen (1987) has suggested that K enrichment in shoshonites can be effected by orthopyroxene-dominated fractionation from a high-alumina basaltic parent at high pressures, producing K enrichment but with little increase in SiO_2. This, however, is contrary to the flat trend defined by the Tibetan data and so K enrichment by fractionation seems unlikely in this case. Experimental results (Edgar *et al.*, 1976; Mengel & Green, 1989) indicate that melts with ~3·5% K_2O are saturated in phlogopite at high pressures. This is slightly lower than the K_2O concentration in the Tibet shoshonites but, allowing for fractionation, is probably similar to the abundance in their parent magmas. We therefore interpret the high K_2O in the Tibet shoshonites as a primary feature, reflecting the presence of a potassic phase, most likely phlogopite, in their source region. This is further supported by the relatively low mantle-normalized abundances of K compared with Th and La in Fig. 7 and the isotope data (see discussion below).

Some trace element trends, such as the positive correlation between Ni and MgO, are probably fractionation related, although many of the incompatible elements do not show the negative correlations predicted by crystal fractionation. For example, the Rb concentration is relatively constant over a range of MgO from 10 to 2%. La shows a negative correlation with MgO within many of the individual sub-area suites but the combined array shows a decrease with MgO (Fig. 6), suggesting that there are important regional variations in the source and degree of melting. The La/Yb ratios are high and variable, and increase with both La and Yb abundances. The low HREE abundances reflect the presence of garnet in the source region, and this can be further illustrated on a diagram of La/Yb vs La (Fig. 10a). Samples from the three geographical regions plot in distinct parts of this diagram. Partial melting models show that a steep trend, in which La/Yb varies from 10 to 170, can only be produced in the presence of residual garnet. Subsequent fractionation increases La abundance whereas La/Yb remains constant, so flat fractionation trends can be easily distinguished from steep partial melting vectors. Thus it is clear from Fig. 10a that the effects of partial melting and source composition were more important than fractional crystallization in controlling the compositional variation within the Tibetan lavas. The southern region lavas define a steep trend with an intercept close to the origin whereas the lavas of the northeastern region fall along a flatter trend but at higher La/Yb ratios. Melting models indicate that such extreme ratios and abundances could not be produced from the

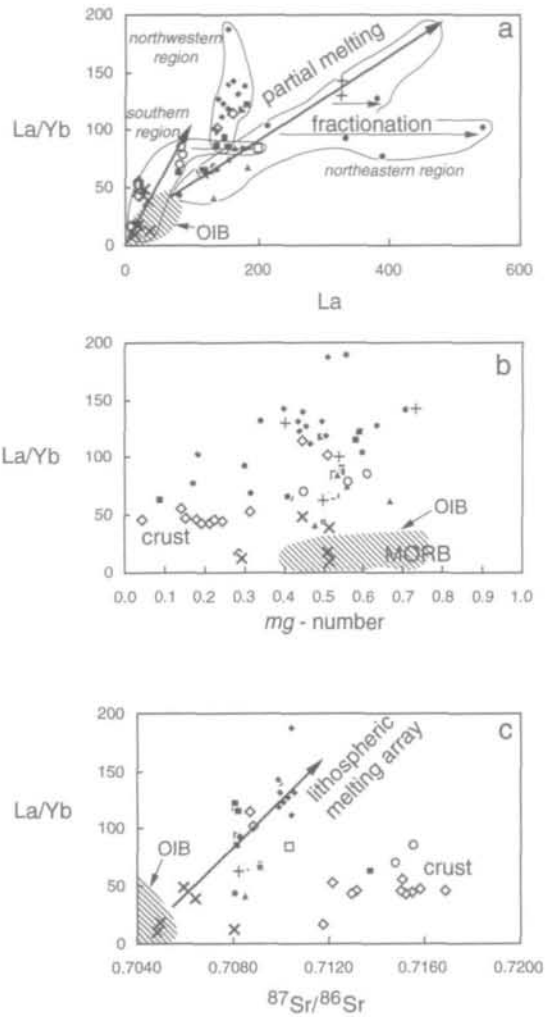

Fig. 10. La/Yb vs La, *mg*-number and $^{87}Sr/^{86}Sr$. The strong positive correlation between La/Yb and La indicates that partial melting (heavy arrows) was the first-order control on the compositional array of the Tibetan lavas, whereas fractionation (light horizontal arrows) played a more minor role. This is unlikely to be a mixing array, because in the mafic lavas there is a large variation in La/Yb at relatively constant *mg*-number and elevated, but restricted $^{87}Sr/^{86}Sr$. Moreover, some of the most primitive lavas (high *mg*-number) have the highest La/Yb and $^{87}Sr/^{86}Sr$. On the La/Yb vs La diagram the individual sub-areas (symbols as in Fig. 5) can be grouped into the three geographical regions which form arrays of different slope, suggesting some variation in their source regions.

same source region as the southern lavas, and this conclusion is supported by the differences in isotope ratios between the northern and southern lavas (see also below). The lavas from the northwestern region do not define a clear trend but show marked variation of La/Yb with little variation in La. They are isotopically similar to those of the northeastern region and so were probably derived from similar source regions, with variations in La/Yb being generated either by different modal abundances of garnet in the source or young regional variations in source composition.

The incompatible element patterns in Fig. 7 have overall concentrations and negative Nb, Ta and Ti anomalies that are unlike those of any oceanic basalt known to be derived from the convecting asthenosphere. Some of these features, such as the negative Nb and Ta anomalies, are observed in crustal rocks, and it is unlikely that the Tibetan magmas could have traversed through some 70 km of crust without assimilating some crustal material. However, the absolute concentrations of incompatible elements (including Nb and Ta) are much higher than those typically observed in crustal rocks, and this makes crustal contamination an improbable origin for these features. Likewise, the extreme concentrations of Nd, Sr and Pb in the lavas mean that the isotope ratios of the lavas are relatively insensitive to contamination. Moreover, the high Ti/Y and low Rb/Ba of most of the mafic lavas are features not generally ascribed to the continental crust and the Tibetan lavas do not lie on simple mixing lines between crust and asthenospheric magmas (Fig. 11). The high abundances of Sr and the lack of significant Eu anomalies indicate that the source was plagioclase free and therefore probably located in the mantle, yet the low Nb/La ratios, radiogenic Sr and Pb and unradiogenic Nd confirm the trace element inferences that this source was distinct from the convecting asthenosphere (Figs 8 and 9). Similarly, the degree of LREE enrichment and fractionation is too great for these magmas to have been generated from a depleted mantle source by a single melting episode. This can be illustrated using the La/Yb ratio as a general measure of the incompatible element enrichment in the Tibetan lavas. For a likely asthenospheric mineralogy and composition, La/Yb will range from 9 to <1 as the degree of melting increases from 1 to 15%, yet La/Yb ranges from 10 to 170 in the Tibetan lavas (Fig. 10a). This range of La/Yb is uncorrelated with *mg*-number; in fact, some of the highest *mg*-number lavas have the highest La/Yb (Fig. 10b), demonstrating that the high La/Yb does not reflect fractionation or combined fractionation and assimilation. In any case, the Ulugh Muztagh and Shiquanhe rhyolites, which would provide likely crustal end-members in such a model, have lower La/Yb and higher $^{87}Sr/^{86}Sr$ than most of the mafic lavas (Fig. 10c). For the mafic lavas themselves $^{87}Sr/^{86}Sr$ is fairly restricted over the large range in La/Yb (Fig. 10c), again suggesting that partial melting, and regional source variations, exerted the dominant control on the minor and trace element variability within the lavas.

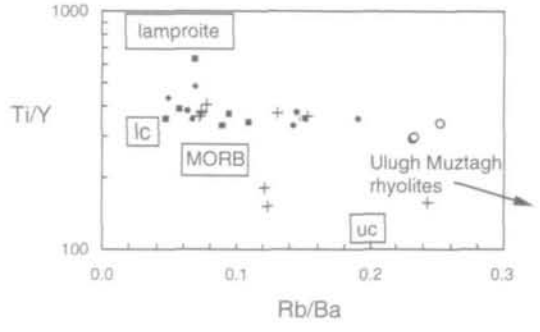

Fig. 11. Plot of Ti/Y vs Rb/Ba, showing that the elemental composition of most of the mafic Tibetan lavas is more akin to small degree mantle melts in equilibrium with residual garnet (represented by lamproites), than crustally contaminated asthenosphere-derived magmas (represented by mixing lines between mid-ocean ridge basalt (MORB) and upper (uc) and lower (lc) crust. Symbols as in Fig. 5.

The most plausible explanation for these combined trace element and isotopic observations on the Tibetan lavas is that they were derived from enriched sub-continental lithospheric mantle. The age of this lithospheric mantle source and its enrichment can be partially constrained by the isotope data. Nd model ages based on a depleted mantle average around 0·9 Ga for the two northern regions. Allowing for a 30% decrease in the Sm/Nd ratio during melting, based on distribution coefficients between melt and a garnet lherzolite assemblage, these ages increase to an average of 1·2 Ga, and range from 0·9 to 1·3 Ga (Table 9). Model ages for the southern region basalts are also around 1·2–1·3 Ga; thus, in general, the Nd isotope ratios indicate a Proterozoic source.

The minimum age at which the Pb isotope system of a sample departed from that of the depleted mantle can be calculated by drawing secondary isochrons from individual Pb isotope data points to the intersection between the geochron and the NHRL (Silver *et al.*, 1988). By contrast with the Nd isotope results, these Pb model ages are mostly Archaean for the Tibetan lavas, ranging from 2·2 Ga for the lavas from the southern region to an average of 3·0 and a maximum of 3·5 in the northern regions. The younger model ages of the southern lavas almost overlap the oldest Nd model ages from this region, but in general the Archaean ages cannot be reconciled with the Proterozoic age recorded by the Nd isotopes and suggest that the source of the Tibetan potassic magmas has had a multi-stage history. Similar observations have been made in other potassic provinces (e.g. Fraser *et al.*, 1986; Rogers *et al.*, 1992) where model ages recorded in volcanic rocks were related to the ages of significant events in the evolution of the local continental lithosphere.

Two-stage modelling of Pb isotopes (following Stacey & Kramers, 1975), assuming a second-stage U/Pb fractionation at 1·2 Ga, indicates that the magma source region originally sustained a slightly low μ ($=^{238}U/^{204}Pb$) environment ($8{\cdot}2 < \mu < 8{\cdot}8$) but following 1·2 Ga, μ increased to values between 12 and 14 (Table 9). Similarly, the high values of $^{208}Pb/^{204}Pb$ relative to the NHRL (Fig. 9b) suggest an increase in κ (Th/U) relative to the bulk Earth value of 3·6. Again assuming Th/U fractionation at 1·2 Ga, the present values of $^{208}Pb/^{204}Pb$ imply a modest increase in κ from 3·6 to 3·8. This compares with an average Th/U ratio in the lavas of 9 and a total range between 7 and 12, implying a dramatic increase in the Th/U ratio during melting, consistent with magma generation by small melt fractions in the presence of garnet (Beattie, 1993). However, the mobility of U during weathering and alteration must also be taken into account, suggesting that the present Th/U ratios may not represent primary values.

Sr model ages based on a depleted mantle and measured Rb/Sr ratios in the lavas are extremely variable and, whereas mean model ages for the three regions are between 1·1 and 1·8 Ga, maximum values may be greater than the age of the Earth. This variability reflects variations in the Rb/Sr ratios of the lavas rather than the $^{87}Sr/^{86}Sr$ ratio, which has a relatively restricted range from 0·705 to 0·711. The Rb/Sr ratio is easily fractionated during magmatic evolution, and this is particularly so in potassic rocks in which phlogopite is a phenocryst phase. Rb/Sr generally increases with SiO_2 in the Tibetan lavas, but in those samples with $<55\%$ SiO_2 it averages 0·072, implying that the primary magmatic value is $<0{\cdot}1$. If Rb/Sr fractionation in the source region is also assumed to have occurred at 1·2 Ga then the measured $^{87}Sr/^{86}Sr$ ratios require an average source Rb/Sr ratio of 0·14, almost double that measured in the least evolved samples and implying that the Rb/Sr ratio was reduced during melting. In an earlier section, it was suggested that the high content of K_2O of $\sim 4\%$ in the majority of the shoshonites implied the presence of a residual potassic phase, possibly phlogopite, in the magma source region. This conclusion is supported by the isotopic arguments presented here which indicate the Rb behaved more compatibly than Sr during melt generation. Moreover, the two-fold fractionation of the Rb/Sr ratio between the source and melt implies a bulk D_{Rb} during melting of $\sim 0{\cdot}2$, assuming D_{Sr} of 0·1. Further assuming that D_{Rb} between phlogopite and melt is 3–3·5 (e.g. Henderson, 1982), this implies a source region with $\sim 6\%$ phlogopite and therefore a K_2O content of $\sim 0{\cdot}6\%$. Such values are

not uncommon in modally metasomatized xenoliths sampled by kimberlites; for example, the PP samples from Erlank *et al.* (1987) range from 0·11 to 2·07% K_2O with an average content of 0·8% K_2O.

In conclusion, the trace element and radiogenic isotope data measured in the Tibetan shoshonites can be reconciled with derivation from a Proterozoic mantle lithospheric source region. Element enrichment at 1·2 Ga resulted in increased U/Pb, Rb/Sr and Th/U, and decreased Sm/Nd ratios relative to depleted mantle, and the stabilization of a phlogopite-bearing mineral assemblage. Nevertheless, the Pb isotope data seem to require an Archaean component, implying a multi-stage history.

DISCUSSION

Although the petrogenetic model presented for the Tibetan volcanism is very general, it places constraints on a diverse range of geological problems ranging from the mechanics of mountain building to climate change, the source of ocean island basalts and the composition of the sub-continental lithospheric mantle.

The composition of the Tibetan sub-continental mantle lithosphere

The implication from the volcanic data is that parts of the Tibetan sub-continental lithospheric mantle were metasomatized and enriched in incompatible trace elements (including volatiles) during the Archaean and Proterozoic and thus must be at least this age themselves. This is in general agreement with the results from studies of mantle xenoliths and many flood basalts (e.g. Waters & Erlank, 1988; Hawkesworth *et al.*, 1990; Turner & Hawkesworth, 1995) and various mechanisms have been proposed for this metasomatism. McKenzie (1989) proposed that the sub-continental lithospheric mantle is semi-continuously being infiltrated by small partial melts from the asthenosphere which introduce volatiles and incompatible elements. However, this enrichment mechanism should equally enrich elements of similar incompatibility and therefore does not provide a mechanism for producing the observed fractionation of Nb, Ta and Ti relative to the rare earths. In other words, it cannot account for the negative Nb–Ta and Ti anomalies in Fig. 7. Such anomalies are characteristics of upper-crustal sediments, and the incorporation of ancient upper-crustal sediments into the source region during a subduction event (e.g. Hergt *et al.* 1989) might also account for the Archaean Pb model ages. However, unless Rb/Ba is strongly fractionated during sediment subduction to leave the sediments with low Rb/Ba, the low Rb/Ba of the majority of the mafic lavas argues (Fig. 11) against such a role for upper-crustal sediment.

Negative Nb–Ta and Ti anomalies are also features of island arc magmas, and it is suggested that ancient subduction processes were responsible for the metasomatism of the Tibetan sub-continental lithospheric mantle. Data from metasomatized sub-arc mantle xenoliths also have negative Ta and Ti anomalies (Maury *et al.*, 1992), providing some support for this model. If this model is correct, it is intriguing that the different terranes which form the Tibetan plateau were accreted during successive Phanerozoic ocean basin closures, because the age of the metasomatism, as indicated by the radiogenic isotope data, is much older than these accretion ages or indeed any of the surficial Tibetan geology, which is dominantly Phanerozoic. The Tibetan lavas further suggest that the Tibetan sub-continental lithospheric mantle is compositionally heterogeneous and geochemical differences between the southern and northern lavas may correspond to different lithosphere being sampled as major terrane boundaries are crossed (see Fig. 15, below).

The source of ocean island basalts

Some ocean island basalts (OIB) require a source which is enriched in incompatible elements, and has ε_{Nd} lower than that of bulk Earth (see Fig. 8). As ancient oceanic crust will never develop $\varepsilon_{Nd} < 0$, it follows that some OIB sources must involve an ancient enriched component. McKenzie & O'Nions (1983, 1995) have suggested that, as the sub-continental lithospheric mantle can preserve geochemical anomalies over long timescales and may be periodically swept back into the asthenospheric convection system (Houseman *et al.*, 1981), the isotope and trace element enrichments in some OIB reflect sampling of pieces of sub-continental lithospheric mantle which have been so removed from beneath orogens such as Tibet. The likely volume of lithospheric mantle removed from beneath Tibet is of the order of 100×10^6 km^3, and the data from the volcanics provide some indication as to what sort of material would be available to OIB sources in such a model.

Some geochemical characteristics of the volcanics, and by implication the Tibetan sub-continental lithospheric mantle, could form an end-member for the OIB arrays (which are shown in Figs 8–10). These include the general enrichment in incompatible elements, elevated LREE/HREE and $^{87}Sr/^{86}Sr$, and low $^{143}Nd/^{144}Nd$. However, other features do

not support the McKenzie & O'Nions model. For example, in Figs 8 and 9, the Tibetan volcanics do not correspond to the EM I, EM II or HIMU compositions proposed as OIB end-members by Zindler & Hart (1986). The Pb isotope data from OIB and MORB define the NHRL (see Fig. 9) and whereas some OIB are displaced above the line (the so-called DUPAL anomaly) it would appear that the Tibetan data are far more enriched in ^{207}Pb and ^{208}Pb, and have too small a range in ^{206}Pb to be an OIB source or end-member. Furthermore, OIB do not exhibit the pronounced negative Ti, Nb and Ta anomalies which are ubiquitous in the Tibetan lavas. Hofmann *et al.* (1986) showed that OIB (and MORB) have high and relatively restricted Ce/Pb (~25) and Nb/U (~47). Figure 12 shows that, in contrast, the Tibetan shoshonites are characterized by much lower Ce/Pb and Nb/U. As Ce/Pb and Nb/U ratios are generally unfractionated during partial melting (Hofmann *et al.*, 1986), and U loss would increase Nb/U, and the Pb contents of the shoshonites are too high for addition of crustal Pb to significantly lower the Ce/Pb ratios, these values are likely to be representative of the lithospheric mantle source of the shoshonites. Metasomatized lithospheric mantle xenoliths also tend to have low Nb/U [see data of O'Reilly & Griffin (1988), Griffin *et al.* (1988) and Maury *et al.* (1992)]; unfortunately, there are no Pb data available from xenoliths to allow us to pursue this model further. Clearly, the lithospheric mantle swept back into the asthenosphere from beneath Tibet was deeper, and it might be argued that it was compositionally distinct, from that which was the source of the volcanics, McKenzie & O'Nions (1995). However, taken at face value, the Tibetan shoshonite data do not appear to provide much support for the source of the Tibetan shoshonites providing OIB end-member.

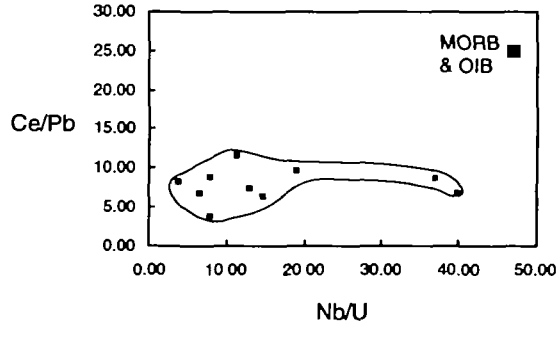

Fig. 12. Ce/Pb vs Nb/U, showing that ocean island basalts [which have high and relatively constant Ce/Pb ~25 and Nb/U ~47; Hofmann *et al.* (1986)] differ markedly from the Tibetan shoshonites, and by inference their lithospheric mantle source region (as Ce/Pb and Nb/U are unlikely to decrease during partial melting). This suggests that the lithospheric mantle that was convectively swept back into the asthenosphere from beneath Tibet is unlikely to be an end-member for ocean island basalts.

Implications for the geodynamic evolution of the India–Asia orogen

The current elevation and extensional deformation of the Tibetan plateau, despite the continuing convergence of India and Asia, have resulted in the plateau becoming the focus of much scientific debate [see Molnar *et al.* (1993) for a comprehensive review]. In a convergent orogen the build-up of topography results in increased gravitational potential energy and extensional buoyancy forces (England & Houseman, 1988, 1989; Sandiford & Powell, 1990; Turner *et al.*, 1992), but, clearly, plate motions can only build up topography to the point where the resultant buoyancy forces balance these driving forces, at which point deformation must cease or be partitioned elsewhere. It follows that extension will only occur if the convergent plate driving forces are reduced or if the topography can be raised by some other means such that the internal buoyancy forces exceed the external driving forces. For these reasons it has been argued that, as there is no evidence for a reduction in the rate of convergence between India and Asia, the current extensional deformation of the Tibetan plateau is best explained by an increase in elevation resulting from removal of part of the underlying lithospheric mantle (England & Houseman, 1988, 1989; Molnar *et al.*, 1993).

The notion that the behaviour of the crust and mantle lithosphere may become decoupled during deformation has major implications for the thermal and mechanical evolution of mountain belts (Houseman *et al.*, 1981; England & Houseman, 1988, 1989; Sandiford & Powell, 1990; Turner *et al.*, 1992; Platt & England, 1994), and it is in the context of these discussions that the potassic volcanism on the Tibetan plateau has particular significance. The coincident onset of extensional deformation and the appearance of widespread, lithospheric mantle-derived volcanism on the plateau appears to mark a major change in tectonic regime. Moreover, the thermal explanation of such magmatism is not straightforward. Melting cannot reflect conductive rebound and radiogenic heating of thickened crust as the low thermal conductivity of rocks means that heating owing to thickening will only develop on the timescale of the thermal time constant of the thickened lithosphere (~240 m.y.). The thickening of the lithosphere and low degrees of extension also rule out the possibility that the magmas reflect decompression melting of the asthe-

nosphere, as this requires that the asthenosphere be brought within 70 km of the surface if a mantle potential temperature of 1280°C is assumed (McKenzie & Bickle, 1988). Given that the areal extent and amount of uplift are large, and yet the magma volumes are small, it seems highly unlikely that the volcanism can be attributed to the effects of a mantle plume. The distribution of the volcanism over an area extending 1000 km north of the arc batholiths rules out a subduction origin; furthermore, magmatism occurred 30 m.y. after collision—a delay which would not be expected if oceanic or continental subduction were the trigger. Moreover, the lavas are shoshonitic not calc-alkaline, and fluid release accompanying subduction provides no thermal rationale for melting within lithospheric mantle that is inferred to already have been metasomatized (volatile enriched).

On the basis of these thermal arguments, Turner *et al.* (1993) concluded that, in Tibet, the only plausible means of attaining temperatures high enough for melting within the lithospheric mantle was to thin it by convection (Figs 13 and 14). The lithospheric mantle is inferred to have undergone an ancient enrichment in incompatible elements and

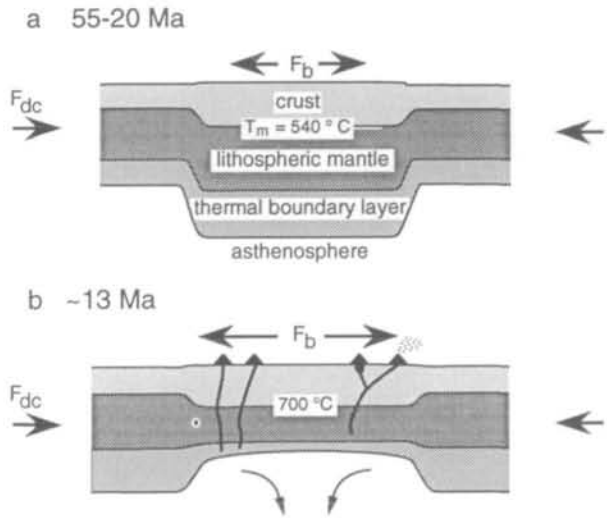

Fig. 13. Diagrammatic illustration of the evolution of a convergent orogen subject to a convergent driving force, F_{dc}, with the resultant development of horizontal buoyancy forces, F_b, that increase with degree of lithospheric thinning from (a) to (b). Before convective thinning of the mantle lithosphere, the maximum elevation of the orogenic plateau is dictated by balance between driving forces and buoyancy forces (a). The increase in potential energy of orogen consequent upon convective thinning of the mantle lithosphere will preclude further compressional deformation (b) and may induce extensional collapse of orogen if buoyancy forces exceed driving force by amount equivalent to strength of the lithosphere to extensional failure. Heating of the lithospheric mantle following thinning causes partial melting of any metasomatized zones to produce potassic volcanism (b). Modified from Turner *et al.* (1992).

volatiles. Before collision, the surface of Tibet had zero elevation, as indicated by Eocene fossiliferous marine limestones (Norin, 1946). Following collision, homogeneous thickening by a factor of two (to obtain 70 km thick crust) resulted in an isostatically supported elevation of 3–4 km. The lithospheric mantle was then thinned by ~60% to achieve the observed 5–5·5 km elevation (Fig. 14), the increase in gravitational potential energy produced by this topography being of the order required to induce extension (England & Houseman, 1988, 1989; Sandiford & Powell, 1990; Turner *et al.*, 1992; Zhou & Sandiford, 1992). Convective thinning of the lithospheric mantle brought previously cooler and insulated zones of the lithospheric mantle into direct contact with asthenospheric temperatures such that any metasomatized peridotite, which had its solidus lowered by the addition of volatiles, underwent partial melting (Fig. 13; Turner *et al.*, 1992). In Fig. 14, the thermal profile after thinning is such that 50% of the lithospheric mantle would have been above the hydrous peridotite solidus and so metasomatized peridotite, insulated when the lithosphere was thick, began to melt. The thermal time constant of the lithosphere is such that gradual conductive heating will continue over a period of ~10–15 m.y. This model is in accordance with the observation that eruptions have continued from ~13 Ma into this century (Liu & Maimaiti, 1989), and seismic evidence for the presence of ~7% partial melt over an 80 km thickness in the upper mantle beneath Tibet (Hirn *et al.*, 1995). Rising Moho temperatures may have promoted crustal melting to produce the Ulugh Muztagh and Shiquanhe rhyolites.

The much larger data base presented here can now be discussed in the context of this general model. For example, any sense of migration of magmatism or spatial–temporal pattern in lava composition could clearly be important in refining the geodynamic models. Figure 15a shows the available age data projected onto a north–south section at 85°E. This suggests that partial melting in the lithospheric mantle beneath Tibet began in the south and rapidly spread northwards towards the present zone of seismic attenuation and inferred high Moho temperatures which also contains the greatest concentration of volcanic rocks (Fig. 1). Assuming the same thermal trigger for the magmatism, this would suggest that convective thinning was initiated in the south and spread northwards. Although limited by the lack of data, Figs 15b and 15c suggest that this northward migration of magmatism was accompanied by decreasing ε_{Nd} and increasing La/Yb, and it is tempting to suggest that the age and/or degree of incompatible element enrichment of the source

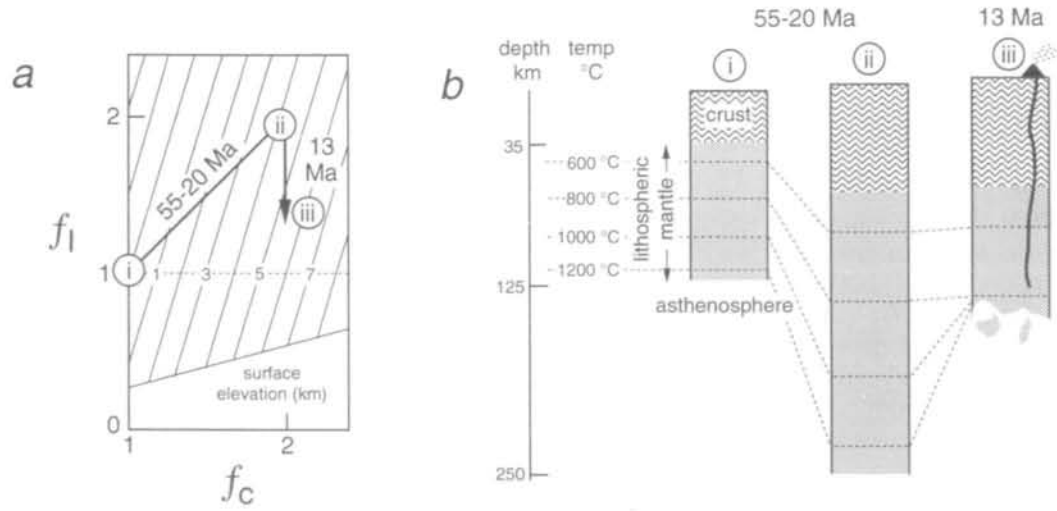

Fig. 14. Thermal and isostatic modelling of a three-stage evolution for the Tibetan plateau, with collisional thickening from (i) to (ii) and thinning of the lithospheric mantle with attendant magmatism and extension from (ii) to (iii). (a) shows an f_c–f_l plane [parameterization and input conditions from Sandiford & Powell (1990) and Turner *et al.* (1992)] contoured for the isostatically compensated surface elevation (see text for explanation). Point (i) represents a crust of normal thickness at sea-level before collision. Homogeneous thickening (f_c=f_l) occurs until (ii), at which time the whole lithosphere is double its original thickness and would have an elevation of 3–4 km. From (ii) to (iii) the mantle lithosphere is thinned (~60%) to obtain its current elevation of 5–5·5 km. This increase in elevation correspondingly increases the gravitational potential energy of the plateau, promoting extensional deformation. A depth–temperature profile for the three stages illustrates the accompanying thermal history in (b). Initially, the lithosphere is of normal thickness and geotherm. Homogeneous thickening from (i) to (ii) moves all material points downwards. Subsequent thinning of the lithospheric mantle compresses the geotherms in the lower portion of the lithospheric mantle and results in metasomatized peridotite in contact with asthenosphere, passing through its solidus and producing shoshonitic volcanism. Conductive heating will result in relaxation of the geotherm on a timescale dictated by the thermal time constant of the lithosphere (~120 Ma) such that volcanism will persist over ~10–15 m.y. (Modified from Turner *et al.*, 1993).

region is greater in the north. It is also noteworthy that the southern lavas erupted through a distinct piece of lithosphere (the Lhasa terrane) compared with the volcanism further north in the Qiantang–Kunlun terranes. It may be that the lithospheric mantle beneath the Lhasa terrane was younger or underwent metasomatic enrichment to a lesser degree and more recently than the terranes further north. A generally lower fertility might also explain the shorter duration of magmatism in the south, and if the metasomatized zone was deeper within the lithosphere it may have heated and undergone partial melting more immediately following convective thinning than shallower levels in the northern terranes.

Unfortunately, the trends in Fig. 15 are largely controlled by the few analyses from the southern region of the plateau, and consequently such musings cannot be placed on a firmer footing until additional samples from the southern region are obtained. The tectonics of the southern plateau and the Himalaya are clearly complex; mineral cooling ages from the Gangdese–Trans Himalaya batholith leave little doubt that there was a rapid increase in exhumation of the Himalaya around 20–17 Ma (Copeland *et al.*, 1987, 1990; Richter *et al.*, 1991; Harrison *et al.*, 1992), which coincides with the increased rate of increase in $^{87}Sr/^{86}Sr$ of seawater ascribed to chemical weathering by Himalayan river systems (Richter *et al.*, 1992; Harris, 1995). We note, however, that despite this exhumation, the lithospheric thicknesses in the Himalaya are likely to prevent decompression melting of the asthenosphere and it is not yet clear how or even if exhumation is linked to the behaviour of the plateau itself.

Cenozoic climate change

High plateaux affect global atmospheric circulation and thus it has been suggested that uplift of the Tibetan plateau may be the cause of intensification of the Asian monsoon, Cenozoic global cooling and increases in Atlantic $\delta^{18}O$ values (Raymo & Ruddiman, 1992; Kutzbach *et al.*, 1993; Molnar *et al.*, 1993). Such hypotheses require geological constraints on the uplift history of the Tibetan plateau. Independent evidence for strengthening of the monsoon between 9 and 6 Ma comes from foraminiferal studies in the Indian Ocean (Kroon *et al.*, 1991) and the carbon-isotope records from the Siwalik Formation (Quade *et al.*, 1989). Subsequent research has attributed isotopic changes observed at

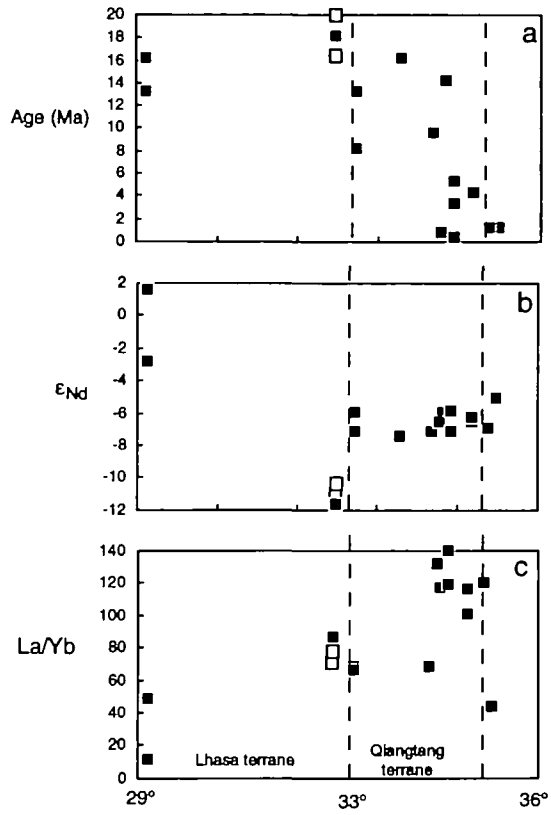

Fig. 15. Representative data from the Tibetan volcanics projected onto a north–south section at 85°E. Although limited by a lack of data from the southern parts of the plateau, it would appear that magmatism migrated from south to north (a), which may suggest that convective thinning of the lithospheric mantle commenced in the south and propagated northwards. The northward migration of volcanism is accompanied by decreases in ε_{Nd} (b) and increases in La/Yb (c), which suggest that the age and/or degree of incompatible element enrichment of the source region is greater in the north. This may reflect differences between the lithospheric mantle beneath the Lhasa terrane and that beneath the Qiangtang, Songban-Ganzi and Kunlun terranes (terrane boundaries indicated by dashed line). Filled squares are shoshonites, open squares are rhyolites.

this time to a global expansion of C4 ecosystems rather than an increased monsoon (Cerling *et al.*, 1993). Molnar *et al.* (1993) proposed that the plateau reached a maximum elevation of ~6 km between 11 and 5 Ma based largely on the dating of normal fault activity, indicating collapse of the plateau following rapid uplift. At the time of writing, this event was determined by reconnaissance data from a single normal fault (Pan & Kidd, 1992), but a second normal fault has now been dated (by ^{40}Ar–^{39}Ar for hydrothermal mica) at 14 Ma (Coleman & Hodges, 1995). Coleman & Hodges (1995) concluded that the plateau reached its high mean elevation well before the Late Miocene.

The present study indicates that convective thinning beneath Tibet had occurred by 13–14 Ma, the earliest period of potassic volcanism on the central plateau. It is possible that southern Tibet underwent slightly earlier uplift and that the onset of uplift migrated northwards, as indicated by older ages from the Maquiang volcanics. We note that at ~13 Ma an increase in $\delta^{18}O$ from 1·2–1·7‰ to >2‰ has been identified from Atlantic Ocean sediments (Raymo & Ruddiman, 1992). Our data are therefore consistent with rapid uplift of the Tibet plateau at ~13 Ma leading to increased chemical weathering rates, downpull of atmospheric CO_2 and global cooling at that time.

ACKNOWLEDGEMENTS

This work represents a compilation of the efforts, thoughts and sample collections of many people. We are particularly grateful to Phil England, Mike Sandiford and John Platt for comments and discussions. Christian Coulon is heartily thanked for providing access to his important sample collection from the southern Tibetan plateau, and both he and Matthew Thirlwall are thanked for their thoughtful reviews, which helped to improve the manuscript. Research at The Open University is partly funded by the NERC, and at URA 10 partly by CNRS–INSU thematic programmes. J. L. thanks the Chinese Academy of Sciences and the British Royal Society for financial assistance.

REFERENCES

Armijo, R., Tapponnier, P., Mercier, J. L. & Tong-Lin, H., 1986. Quaternary extension in southern Tibet: field observations and tectonic implications. *Journal of Geophysical Research* **91**, 13803–13872.

Arnaud, N. O., 1992. Apport de la thermochronologie $^{40}Ar/^{39}Ar$ sur feldspath potassique connaissance de la tectonique cénozoïque d'Asie. Ph.D. Thesis, Université de Clermont-Ferrand 2, 300 pp.

Arnaud, N. O., Vidal, Ph., Tapponnier, P., Matte, Ph. & Deng, W. M., 1992. The high K_2O volcanism of northwestern Tibet: geochemistry and tectonic implications. *Earth and Planetary Science Letters* **111**, 355–367.

Beattie, P., 1993. Uranium–thorium disequilibria and partitioning on melting of garnet peridotite. *Nature* **363**, 63–65.

Brandon, C. & Romanovitz, B., 1986. A 'no lid' zone in the central Chang-Thang platform of Tibet: evidence from pure path phase velocity measurements of long-period Rayleigh waves. *Journal of Geophysical Research* **91**, 6547–6564.

Burchfiel, B. C., Molnar, P., Ziyua, Z., K'uangyi, L., Shuji, W., Miumin, H. & Sutter, J., 1989. Geology of the Ulugh Muztagh area, Northern Tibet. *Earth and Planetary Science Letters* **94**, 57–70.

Cerling, T. E., Wang, Y. & Quade, J., 1993. Expansion of C4 ecosystems as an indicator of global ecological change in the Late Miocene. *Nature* **361**, 344–345.

Coleman, M. & Hodges, K., 1995. Evidence for Tibetan plateau uplift before 14 Myr ago from a new minimum age for east–west extension. *Nature* **374**, 49–52.

Copeland, P., Harrison, T. M., Kidd, W. S. F., Ronghua, X. & Yuquan, Z., 1987. Rapid early Miocene acceleration of uplift in the Gangdese Belt, Xizung (southern Tibet) and its bearing on accommodation mechanisms of the India–Asia collision. *Earth and Planetary Science Letters* **86,** 240–252.

Copeland, P., Harrison, T. M. & Heizler, M. T., 1990. $^{40}Ar/^{39}Ar$ single-crystal dating of detrital muscovite and K-feldspar from Leg 116, southern Bengal fan: implications for the uplift and erosion of the Himalayas. *Proceedings Ocean Drilling Program, Scientific Results* **116.** College Station, TX: Ocean Drilling Program, pp. 93–114.

Coulon, C., Maluski, H., Bollinger, C. & Wang, S., 1986. Mesozoic and Cenozoic volcanic rocks from central and southern Tibet: $^{40}Ar/^{39}Ar$ dating, petrological characteristics and geodynamical significance. *Earth and Planetary Science Letters* **79,** 281–302.

Debon, F., Le Fort, P., Sheppard, S. M. F. & Sonet, J., 1986. The four plutonic belts of the Transhimalaya: a chemical, mineralogical, isotopic and chronological synthesis along a Tibet–Nepal section. *Journal of Petrology* **27,** 219–250.

Deng, W. M., 1989*a*. Cenozoic volcanic rocks in the northern Ngari district of the Tibet (Xizang). Discussion on the concurrent intracontinental subduction. *Acta Petrologica Sinica* **3.**

Deng, W. M., 1989*b*. Volcanism in Tibet. *Journal of Natural Resources* **3,** 205–210.

Dewey, J., Shackelton, R. M., Chang, C. & Sun, Y., 1988. The tectonic evolution of the Tibetan plateau. *Philosophical Transactions of the Royal Society of London* **A327,** 379–413.

Edgar, A. D., Green, D. H. & Hibberson, W. O., 1976. Experimental petrology of a highly potassic magma. *Journal of Petrology* **17,** 339–356.

England, P. C. & Houseman, G. A., 1988. The mechanics of the Tibetan plateau. *Philosophical Transactions of the Royal Society of London* **A326,** 301–319.

England, P. C. & Houseman, G. A., 1989. Extension during continental convergence, with application to the Tibetan Plateau. *Journal of Geophysical Research* **94,** 17561–17579.

Erlank, A. J., Waters, F. G., Hawkesworth, C. J., Haggerty, S. E., Allsopp, H. L., Rickard, R. S. & Menzies, M. A., 1987. Evidence for mantle metasomatism in peridotite nodules from the Kimberley Pipes, South Africa. In: Menzies, M. A. & Hawkesworth, C. J. (eds) *Mantle Metasomatism.* London: Academic Press, pp. 221–311.

France-Lanord, C. & Le Fort, P., 1988. Crustal melting and granite genesis during the Himalayan collision orogenesis. *Transactions of the Royal Society of Edinburgh* **79,** 183–196.

Fraser, K. J., Hawkesworth, C. J., Erlank, A. J., Mitchell, R. H. & Scott-Smith, B. H., 1986. Sr, Nd and Pb isotope and minor element geochemistry of lamproites and kimberlites. *Earth and Planetary Science Letters* **76,** 57–70.

Fuhrman, M. L. & Lindsley, D. H., 1988. Ternary feldspar modeling and thermometry. *American Mineralogist* **73,** 201–215.

Griffin, W. L., O'Reilly, S. Y. & Stabel, A., 1988. Mantle metasomatism beneath western Victoria, Australia: II. Isotopic geochemistry of Cr-diopside lherzolites and Al-augite pyroxenites. *Geochimica et Cosmochimica Acta* **52,** 449–459.

Harris, N. B. W., 1995. Significance of weathering Himalayan metasedimentary rocks and leucogranites for the Sr-isotope evolution of seawater during the Early Miocene. *Geology* **23,** 795–798.

Harris, N. B. & Massey, J., 1994. Decompression and anatexis of Himalayan metapelites. *Tectonics* **13,** 1537–1546.

Harris, N. B. W., Pearce, J. A. & Tindle, A. G., 1986. Geochemical characteristics of collision-zone magmatism. In: Coward, M. P. & Ries, A. C. (eds) *Collision Tectonics. Geological Society of London Special Publication* **19,** 67–82.

Harris, N. B. W., Ronghua, X., Lewis, C. L. & Chengwei, J., 1988*a*. Plutonic rocks of the 1985 Tibet Geotraverse, Lhasa to Golmud. *Philosophical Transactions of the Royal Society of London* **A327,** 145–168.

Harris, N. B., Ronghua, X., Lewis, C. L., Hawkesworth, C. J. & Yuquan, Z., 1988*b*. Isotope geochemistry of the 1985 Tibet Geotraverse, Lhasa to Golmud. *Philosophical Transactions of the Royal Society of London* **A327,** 263–285.

Harrison, T. M., Copeland, P., Kidd, W. S. & Yin, A., 1992. Raising Tibet. *Science* **255,** 1663–1670.

Hawkesworth, C. J., Kempton, P. D., Rogers, N. W., Ellam, R. M. & van Calsteren, P. W., 1990. Continental mantle lithosphere, and shallow level enrichment processes in the Earth's mantle. *Earth and Planetary Science Letters* **96,** 256–268.

Henderson, P., 1982. *Inorganic Geochemistry.* Oxford: Pergamon Press, 353 pp.

Hergt, J. M., Chappell, B. W., McCulloch, M. T., McDougall, I. & Chivas, A. R., 1989. Geochemical and isotopic constraints on the origin of the Jurassic dolerites of Tasmania. *Journal of Petrology* **30,** 841–883.

Hirn, A., Jiang, M., Sapin, M., Diaz, J., Nercessian, A., Lu, Q. T., Lépine, J. C., Shi, D. N., Sachpazi, M., Pandey, M. R., Ma, K. & Gallart, J., 1995. Seismic anisotropy as an indicator of mantle flow beneath the Himalayas and Tibet. *Nature* **375,** 571–574.

Hofmann, A. W., Jochum, K. P., Seufert, M. & White, W. M., 1986. Nb and Pb in oceanic basalts: new constraints on mantle evolution. *Earth and Planetary Science Letters* **79,** 33–45.

Houseman, G. A. & England, P., 1994. Crustal thickening versus lateral expulsion in the Indian–Asian continental collision. *Journal of Geophysical Research* **98,** 12233–12250.

Houseman, G. A., McKenzie, D. P. & Molnar, P. J., 1981. Convective instability of a thickened boundary layer and its relevance for the thermal evolution of continental convergent belts. *Journal of Geophysical Research* **86,** 6115–6132.

Jin, Y., McNutt, M. K. & Zhu, Y., 1994. Evidence from gravity and topography data for folding of Tibet. *Nature* **371,** 669–674.

Kidd, W. S. & Molnar, P., 1988. Quaternary and active faulting observed on the 1985 Academia Sinica–Royal Society Geotraverse of Tibet. *Philosophical Transactions of the Royal Society of London* **A327,** 337–363.

Kroon, D., Steens, T. & Troelstra, S. R., 1991. Onset of monsoonal related upwelling in the western Arabian Sea as revealed by planktonic foraminifera. *Proceedings Ocean Drilling Program, Scientific Results* **117.** College Station, TX: Ocean Drilling Program, pp. 257–263.

Kutzbach, J. E., Prell, W. L. & Ruddiman, W. F., 1993. Sensitivity of Eurasian climate to surface uplift of the Tibetan plateau. *Journal of Geology* **101,** 177–190.

Li, J.-J., Li, B.-Y., Wang, F. B., Zhang, Q. S., Wen, S. X. & Zheng, B.-X., 1981. The process of the uplift of the Qinghai-Xizang plateau. In: Liu, D.-S. (ed.) *Geological and Ecological Studies of Qinghai-Xizang Plateau.* Beijing: Science Press, pp. 111–118.

Lindsley, D. H., 1983. Pyroxene thermometry. *American Mineralogist* **68,** 477–493.

Liu, J. & Maimaiti, Y., 1989. Distribution and ages of Ashikule volcanoes on the West Kunlun Mountains, west China. *Bulletin of Glacial Research* **7,** 187–190.

Maluski, H., Matte, P. & Brunel, M., 1988. Argon 39–Argon 40 dating of metamorphic events in the north and high Himalaya belts (southern Tibet–China). *Tectonics* **7**, 299–326.

Maury, R. C., Defant, M. J. & Joron, J-L., 1992. Metasomatism of the sub-arc mantle inferred from trace elements in Philippine xenoliths. *Nature* **360**, 661–663.

McKenna, L. W. & Walker, J. D., 1990. Geochemistry of crustally derived leucocratic igneous rocks from the Ulugh Muztagh area, Northern Tibet, and their implications for the formation of the Tibetan Plateau. *Journal of Geophysical Research* **95**, 21483–21502.

McKenzie, D., 1989. Some remarks on the movement of small melt fractions in the mantle. *Earth and Planetary Science Letters* **95**, 53–72.

McKenzie, D. P. & Bickle, M. J., 1988. The volume and composition of melt generated by extension of the lithosphere. *Journal of Petrology* **29**, 625–679.

McKenzie, D. & O'Nions, R. K., 1983. Mantle reservoirs and ocean island basalts. *Nature* **301**, 229–231.

McKenzie, D. & O'Nions, R. K., 1995. The source regions of ocean island basalts. *Journal of Petrology* **36**, 133–159.

Meen, J. K., 1987. Formation of shoshonites from calc-alkaline basalt magmas: geochemical and experimental constraints from the type locality *Contributions to Mineralogy and Petrology* **97**, 333–351

Mengel, K. & Green, D. H., 1989. Stability of amphibole and phlogopite in metasomatised peridotite under water-saturated and water-undersaturated conditions. In: *Kimberlites and Related Rocks, Vol 1. Special Publication, Geological Society of Australia* **14**, 571–581.

Mercier, J-L., Armijo, R., Tapponnier, P., Carey-Gailhardis, E. & Tong Lin, H., 1987. Change from Late Tertiary compression to Quaternary extension in southern Tibet during the India–Asia collision. *Tectonics* **6**, 275–304.

Molnar, P., 1988. A review of geophysical constraints on the deep structure of the Tibetan Plateau, the Himalaya and the Karakoram, and their tectonic implications. *Philosophical Transactions of the Royal Society of London* **A326**, 33–88.

Molnar, P, 1990. S-wave residuals from earthquakes in the Tibetan region and lateral variations in the upper mantle. *Earth and Planetary Science Letters* **101**, 68–77.

Molnar, P., England, P. & Martinod, J., 1993. Mantle dynamics, uplift of the Tibetan plateau and the Indian Monsoon. *Reviews in Geophysics* **31**, 357–396.

Norin, E., 1946. *Geological Explorations in Western Tibet, Reports from the Scientific Expedition to the Northwestern Provinces under the Leadership of Dr Sven Hedin*. Stockholm; Tryckeri Aktiebolaget, 29, Part 3, Geology 7.

O'Reilly, S Y. & Griffin, W. L., 1988. Mantle metasomatism beneath western Victoria, Australia: I. Metasomatic processes in Cr-diopside lherzolites. *Geochimica et Cosmochimica Acta* **52**, 433–447.

Pan, Y. & Kidd, W. S. F., 1992. Nyainqentanglha shear zone: a late Miocene extensional detachment in the southern Tibetan Plateau. *Geology* **20**, 775–778.

Pearce, J. A. & Mei, H., 1988. Volcanic rocks of the 1985 Geotraverse: Lhassa to Golmud. *Philosophical Transactions of the Royal Society of London* **A327**, 169–201.

Pearce, J. A., Harris, N. B. & Tindle, A. G., 1984. Trace element discrimination diagrams for the tectonic interpretation of granitic rocks. *Journal of Petrology* **25**, 956–983.

Peccerillo, A. & Taylor, D. R., 1976. Geochemistry of Eocene calc-alkaline volcanic rocks from the Kastamonu area, Northern Turkey. *Contributions to Mineralogy and Petrology* **58**, 63–91.

Platt, J. P. & England, P. C., 1994. Convective removal of lithosphere beneath mountain belts: thermal and mechanical consequences. *American Journal of Science* **294**, 307–336.

Quade, J., Cerling, T. E. & Bowman, J. R., 1989. Development of Asian monsoon revealed by marked ecological shift during the latest Miocene in northern Pakistan. *Nature* **342**, 163–166.

Raymo, M. E. & Ruddiman, W. F., 1992. Tectonic forcing of late Cenozoic climate. *Nature* **359**, 117–122.

Richter, F. M., Lovera, O. M., Harrison, T. M. & Copeland, P., 1991. Tibetan tectonics from $^{40}Ar/^{39}Ar$ analysis of a single K-feldspar sample. *Earth and Planetary Science Letters* **105**, 266–278.

Richter, F. M., Rowley, D. B. & DePaolo, D. J., 1992. Sr isotope evolution of seawater: the role of tectonics. *Earth and Planetary Science Letters* **109**, 11–23.

Rogers, N. W., de Mulder, M. & Hawkesworth, C. J., 1992. An enriched mantle source for potassic basanites: evidence from Karisimbi volcano, Virunga volcanic province, Rwanda. *Contributions to Mineralogy and Petrology* **111**, 543–556.

Sandiford, M. & Powell, R., 1990. Some isostatic and thermal consequences of the vertical strain geometry in convergent orogens. *Earth and Planetary Science Letters* **95**, 85–96.

Shackelton, R. M. & Chang, C., 1988. Cenozoic uplift and deformation of the Tibetan Plateau: the geomorphological evidence. *Philosophical Transactions of the Royal Society of London* **A327**, 365–377.

Silver, P. G., Carlson, R. W. & Olson, P., 1988. Deep slabs, geochemical heterogeneity, and the large-scale structure of mantle convection: investigation of an enduring paradox. *Annual Review of Earth and Planetary Sciences* **16**, 477–542.

Stacey, J. S. & Kramers, J. D., 1975. Approximation of terrestrial lead isotope evolution by a two-stage model. *Earth and Planetary Science Letters* **26**, 207–221.

Sun, S-s. & McDonough, W. F., 1989. Chemical and isotopic systematics of oceanic basalts: implications for mantle composition and processes. In: Saunders, A. D. & Norry, M. J. (eds) *Magmatism in Ocean Basins. Geological Society of London Special Publication* **42**, 313–345.

Turner, S. & Hawkesworth, C., 1995. The nature of the sub-continental mantle: constraints from the major element composition of continental flood basalts. *Chemical Geology* **120**, 295–314.

Turner, S. P., Sandiford, M. & Foden, J. D., 1992. Some geodynamic and compositional constraints on 'post orogenic' magmatism. *Geology* **20**, 931–934.

Turner, S., Hawkesworth, C. J., Liu, J., Rogers, N., Kelley, S. & van Calsteren, P., 1993. Timing of Tibetan uplift constrained by analysis of volcanic rocks. *Nature* **364**, 50–53.

Waters, F. G. & Erlank, A. J., 1988. Assessment of the vertical extent and distribution of mantle metasomatism below Kimberley, South Africa. *Journal of Petrology, Special Volume* 185–204.

Zhou, S. & Sandiford, M., 1992. On the stability of isostatically compensated mountain belts. *Journal of Geophysical Research* **97**, 14207–14223.

Zindler, A. & Hart, S., 1986. Chemical geodynamics. *Annual Review of Earth and Planetary Sciences* **14**, 493–571.

RECEIVED MARCH 30, 1995
REVISED TYPESCRIPT ACCEPTED JULY 18, 1995